CHARACTERIZATION OF ZEOLITES AND ZEOTYPES

By

SÍLVIA CLÁUDIA LOUREIRO DIAS

A DISSERTATION PRESENTED TO THE GRADUATE SCHOOL
OF THE UNIVERSITY OF FLORIDA IN PARTIAL FULFILLMENT
OF THE REQUIREMENTS FOR THE DEGREE OF
DOCTOR OF PHILOSOPHY

UNIVERSITY OF FLORIDA

1997

This work is dedicated to my husband, whose love and faith in me were stronger than my own; without him, this work would never have come to pass. I also dedicate this dissertation to my family for their constant support.

ACKNOWLEDGMENTS

I would like to thank the many people who have helped me throughout my carreer here at the University of Florida. Foremost, I would like to express my gratitude to my research advisor, Russell S. Drago, for helping me to come to the University of Florida and for teaching me much more than I would ever be able to thank him for. I would equally like to thank Ruth Drago whose hospitality helped a lot during these years. Maribel Lisk also deserves special thanks. Her friendship and assistance have been most appreciated.

On a personal note, there are a few people I would like to mention. I would like to acknowledge one person specifically who has had the greatest impact on my life. This recognition goes to my husband, José A. Dias. It has been through his constant support, love and by his own example that I have been successful in what I have undertaken. Most importantly, I would like to thank my family. My father and mother, Ubatan and Maria Loureiro, for their weekly supporting phone calls from Brazil. They did everything so that I could have and attain the best. They taught me by example that I could do anything with hard work and determination. I would also like to thank my brother, sister, sister-in law and parents-in-law for constant prayers and support. To my family and friends for

their prayers and calls, my deepest thanks and eternal gratitude. Finally, I would like to thank Dr. Sandra Diaz for her uncountable help during difficult moments.

I would also like to thank the Conselho Nacional de Desenvolvimento Científico e Tecnológico (CNPq) for the grant (proc. 200870/93-9) of a scholarship for pursuing Ph.D. at the University of Florida and the Universidade de Brasília (Brazil) for the leave of absence during this period.

There are people who should be noted for their contributions: Dr. Kathryn Williams (University of Florida) for carrying out TGA and NAA, Dr. Geraldo Boaventura (Universidade de Brasília, Brazil) for carrying out ICP and AAS, and Dr. Mariana Torrealba (Intevep, Venezuela) for carrying out NMR analysis. No acknowledgment could be complete without mention of the people with whom I work everyday (the Drago group).

TABLE OF CONTENTS

page

ACKNOWLEDGMENTS....iii

LIST OF TABLES....vii

LIST OF FIGURES....viii

ABSTRACT....xi

CHAPTER 1: INTRODUCTION TO ZEOLITES....1

CHAPTER 2: INVESTIGATION OF ACIDITY OF HZSM-5....18

Introduction....18
Experimental....22
Results and Discussion....30
Conclusion....60

CHAPTER 3: ACIDITY OF TS-1....62

Introduction....62
Experimental....67
Results and Discussion....68
Conclusion....79

CHAPTER 4: MEASUREMENTS OF ACIDITY OF Y ZEOLITES....80

Introduction....80
Experimental....85
Results and Discussion....89
Conclusion....106

LIST OF REFERENCES....107

BIOGRAPHICAL SKETCH.....114

LIST OF TABLES

Table page

1-1. Developments in Zeolite Science and Technology....2

1-2. Size of Cavities and Pore Structure of Some Zeolites....8

1-3. Critical Molecular Sizes....9

1-4. Main Commercial Processes Involving Zeolites....12

2-1. Hypothetical Illustration of Moles Adsorbed at Two Competing Sites as a Function of K and n....43

2-2. Thermodynamic Parameters Obtained in Hexane Solvent for Reactions of HZSM-5 (Bulk Si/Al of 36) with Pyridine, 2,6-Lutidine and 2,6-di-t-butylpyridine....46

3-1. Thermodynamic Parameters Obtained in Hexane Solvent for Reactions of TS-1 (1%Ti) with Pyridine and 2,6-Lutidine....76

4-1. Reported properties of Y zeolites....87

4-2. ICP and NA analysis for Y zeolites....90

4-3. AAS analysis for Y zeolites....90

4-4. Elemental Analysis of Y zeolites....91

4-5. Thermodynamic Parameters for Reactions of Y Zeolite with Pyridine, 2,6-Lutidine, 2,6-di-t-butylpyridine, Quinoline, Tetrahydrothiophene, and Benzonitrile....102

4-6. E and C Fit for the Most Acidic Sites on Y Zeolite....105

LIST OF FIGURES

Figure page

1-1. Basic Building Blocks of Zeolites-Molecular Sieves....6

1-2. Representation of the Types of Shape Selectivity Exhibited by Zeolites....13

2-1. (a) Framework Topology and Symmetry Elements of the (010) Pentasil Layer in ZSM-5 (MFI). The 12T-atom Building Unit is shown by bold lines; (b) (100) Pentasil Layer in Pnma (As-synthesized or High Temperature) ZSM-5; (c) Representation of the Channel System in ZSM-5....19

2-2. Calorimetric Aparattus....24

2-3. Adsorption Aparattus....25

2-4. FTIR Spectra in Nujol Mulls of HZSM-5 (a) as Received and (b) After Drying at 450 °C in Vacuum....33

2-5. FTIR Spectra in Nujol Mulls of HZSM-5 (a) Dried and (b) After Calorimetric Titration with Pyridine....33

2-6 (a). ^{1}H NMR Spectrum of Solid HZSM-5. $\delta = 4.0$ ppm (bridging hydroxyl AlOH), $\delta = 2.5$ ppm (extra-framework AlOH) and $\delta = 1.7$ ppm (silanol groupsOH)....34

2-6 (b). ^{27}Al NMR Spectrum of Solid HZSM-5. $\delta = 54$ ppm (tetra-coordinated framework Al), $\delta = 0$ ppm (hexa-coordinated extra-framework Al)....35

2-6 (c). ^{29}Si NMR Spectrum of Solid HZSM-5. $\delta = 117.0$ and 113.2 ppm (non-equivalent Si atoms bonded to other Si)....36

2-7. Adsorption Isotherm and Heat of Adsorption versus Concentration of Pyridine in Solution: (■) Calorimetric Points, (●) Adsorption Data Points, and (—) Solid Line: Calculated Using Values from Table 2-2....38

2-8. Adsorption Isotherm and Heat of Adsorption versus Concentration of 2,6-Lutidine

in Solution: (■) Calorimetric Points, (●) Adsorption Data Points, and (—) Solid Line: Calculated Using Values from Table 2-2.....39

2-9. Adsorption Isotherm and Heat of Adsorption versus Concentration of 2,6-di-tert-butylpyridine in Solution: (■) Calorimetric Points, (●) Adsorption Data Points, and (—) Solid Line: Calculated Using Values from Table 2-2.....40

2-10. Average Enthalpies of Reactions versus mmol of Base Added. (●) pyridine (■) 2,6-Lutidine, (▲) 2,6-di-tert-butylpyridine.....42

2-11. Sum of Heat Evolved versus Concentration of Pyridine in Solution for Two Acid Sites: (■) Calorimetric Data Points,(--) Dashed Line: Process 1 (first site), Bold Line: Process 2 (second site), and (■) Solid Line: Calculated using Values from Table 2-2.....48

2-12. Adsorption Isotherm versus Concentration of Pyridine in Solution: (■) Adsorption Data Points,(--) Dashed Line: Process 1 (first site), Bold Line: Process 2 (second site), and (■) Solid Line: Calculated using Values from Table 2-2.....50

3-1. Crystalline Structure of TS-1.....63

3-2. FTIR Spectra in Nujol Mulls of TS-1 (a) as Received and (b) After Drying at 400 °C in Vacuum.....69

3-3. FTIR Spectra in Nujol Mulls of TS-1 (a) Dried and (b) After Calorimetric Titration with Pyridine.....70

3-4. FTIR Spectra in Nujol Mulls of (a) TS-1 and (b) HZSM-5 Dried.....72

3-5. Adsorption Isotherm and Heat of Adsorption versus Concentration of Pyridine in Solution: (■) Calorimetric Points, (●) Adsorption Data Points, and (—) Solid Line: Calculated Using Values from Table 3-1.....73

3-6. Adsorption Isotherm and Heat of Adsorption versus Concentration of 2,6-Lutidine in Solution: (■) Calorimetric Points, (●) Adsorption Data Points, and (—) Solid Line: Calculated Using Values from Table 3-1.....74

3-7. Average Enthalpies of Reactions versus Mmol of Base added. (■) Pyridine, (▲) 2,6-Lutidine.....75

3-8. Sum of Heat Evolved versus Concentration of Pyridine in Solution for Two Acid Sites: (■) Calorimetric Data Points,(--) Dashed Line (under solid line): Site 1 and Bold Line: Site 2. Solid Line: Calculated using Values from Table 3-1.....77

4-1. Faujasite framework showing oxygen types (O).....82

4-2. Drying Aparattus Used for Calcination of Samples.....86

4-3. TGA Plot of Y Zeolite (Si/Al = 2.7) from bottle.....92

4-4. TGA Plot of Y Zeolite (Si/Al = 3.0) from bottle.....92

4-5. TGA Plot of Y Zeolite (Si/Al = 6.8) from bottle.....93

4-6. TGA Plot of Y Zeolite (Si/Al = 50) from bottle.....93

4-7. XRD Plot of Y Zeolite (Si/Al = 3.0) Dried at 450 °C.....94

4-8. XRD Plot of Y Zeolite (Si/Al = 50) Dried at 450 °C.....94

4-9. XRD Plot of Y Zeolite (Si/Al = 6.8) from Bottle.....95

4-10. XRD Plot of Y Zeolite (Si/Al = 6.8) Dried at 450 °C.....95

4-11. FTIR Spectra of Y Zeolite (Si/Al = 2.7) from (a) bottle and (b) Dried at 450 °C...97

4-12. FTIR Spectra of Y Zeolite (Si/Al = 3.0) from (a) bottle and (b) Dried at 450 °C...97

4-13. FTIR Spectra of Y Zeolite (Si/Al = 6.8) from (a) bottle and (b) Dried at 450 °C...98

4-14. FTIR Spectra of Y Zeolite (Si/Al = 50) from (a) bottle and (b) Dried at 450 °C....98

4-15. FTIR Spectra of Y Zeolite (Si/Al = 3.0) (a) Dried at 450 °C and (b) after Deuteration.....99

4-16. FTIR Spectra of Y Zeolites After Calorimetric Experiment (a). Si/Al = 2.7; (b). Si/Al = 6.8; (c). Si/Al = 3.0.....99

4-17. Heats of Adsorption of Pyridine for Y Zeolites (□ Si/Al = 3.0), (● Si/Al = 6.8) and (▲ Si/Al = 50).....101

4-18. Isotherms of Adsorption of Pyridine for Y Zeolites (● Si/Al = 3.0), (■Si/Al = 6.8) and (▲ Si/Al =50).....101

4-19. Representation of Y zeolite. The corners denote the positions of the T atoms (T = Si or Al) and the lines represent the bridging oxygen atoms. The small pictures show the 4 different positions of the protons that are covalently bonded to the oxygen atoms around an aluminum atom.....104

Abstract of Dissertation Presented to the Graduate School
of the University of Florida in Partial Fulfillment of the
Requirements for the Degree of Doctor of Philosophy

CHARACTERIZATION OF ZEOLITES AND ZEOTYPES

By

Silvia C. Dias

December 1997

Chairman: Russell S. Drago
Major Department: Chemistry

The purpose of this work is the employment of combined analysis for evaluating the acidity of solids. Solid acid catalysts are the most commonly used catalytic materials in the chemical industry. Amongst solid acids, zeolites are most important in commercial processes including water treatment and cracking of hydrocarbons.

The combined analysis of calorimetric and adsorption data, cal-ad analysis, provides a novel characterization of the donor-acceptor properties of these solid acids. Of all studies to date, only cal-ad provides a measure of the extent, K_i ; strength, ΔH_i ; and quantity of acid sites, n_i. The reaction of HZSM-5 with pyridine shows 0.0415 mmol per g of a strong Brönsted site ($-\Delta H_1 = 42.1$ kcal mol^{-1}) and 0.53 mmol per g of a hydrogen bonding site ($-\Delta H_2 = 8.6$ kcal mol^{-1}). Titrations with 2,6-lutidine and 2,6-di-*tert*-

butylpyridine indicate that the strong Brönsted sites are located in the 5.5 Å channels with no detectable amounts on the exterior surface.

TS-1 is used in a variety of oxidation reactions of organic substrates with H_2O_2. The cal-ad data of TS-1 with pyridine shows the absence of the strong acid site found in HZSM-5 and the presence of only 0.07 mmol per g of a -15.1 kcal mol^{-1} hydrogen bonding site. The small amount of these sites, 0.07 mmol per g compared to 0.5 mmol for the hydrogen bonding sites of HZSM-5 accounts for the lower affinity of TS-1 for water.

Cal-ad studies of Y zeolite with pyridine and 2,6-lutidine show 0.108 and 0.106 mmol per g of a Brönsted site, respectively ($-\Delta H_2$ = 34.1 and 30.8 kcal mol^{-1}, respectively) inside the large cages of the solid. The results also indicate 0.2 mmol per g of hydrogen bonding sites ($-\Delta H_2$ = 17.7 kcal mol^{-1}) on the interior and exterior surface of the zeolite.

Enthalpies of reactions of Y zeolite with pyridine, quinoline, tetrahydrothiophene, and benzonitrile for the strongest sites were well fit to the ECW model leading to a large amount of covalent character (C_A/E_A = 1.31) in the donor-acceptor interactions.

CHAPTER 1
INTRODUCTION TO ZEOLITES

In 1756, the discovery of a new class of silicate minerals was reported by the Swedish mineralogist Axel Fredrick Cronstedt (1722-1765). As he described, these minerals "exhibit so strange and peculiar behavior in a blowpipe flame that they are impossible to identify with any known family."[1] The two samples he examined from Iceland and Finland emitted gas and puffed up like borax when heated in the blowpipe flame. He named these minerals zeolites from the Greek words "zeo" (boiling) and "litos" (stone) meaning a material able to eliminate large amounts of water when heated. For almost 200 years zeolites remained an obscure group of minerals with rather unusual properties, and Cronstedt was remembered primarily for his discovery of the element nickel.

Cronstedt would probably have found it difficult to believe that synthetic analogs of the mineral group he described would play a major role in processing fuels and synthetic materials for our 20th century world. The significance of zeolites is best understood when placed in the historical context of their development, as is summarized in Table 1-1.[2]

Table 1-1. Developments in Zeolite Science and Technology.

Early History		
1756	A.F. Cronstedt	described natural zeolites
1840	A. Damour	observed reversible dehydration
1858	H. Eichhorn	reported ion-exchange properties of zeolites
1862	H. de St. Claire-Deville	early hydrothermal synthesis (levyne)
1876	Lew	reported sedimentary zeolites in tuff deposit
1896	G. Friedel	observed organic liquid sorption; proposed open spongy framework structure
1909	F. Grandjean	reported gas sorption (NH_3, air, H_2)
1925	O. Weigel & F. Steinhoff	observed molecular sieve effect
1930	W.H. Taylor/ L. Pauling	structure determinations of analcime/natrolite
1932-45	R.M. Barrer	studies of synthesis, ion-exchange sorption, and dehydration
Industrial Era		
1949-54	Union Carbide	synthesis of zeolite A and zeolite X (faujasite)
1954	Union Carbide	commercialized zeolite-based gas purification and separation processes; early catalytic applications
1955-62	Mobil	commercialized rare earth zeolite X cracking catalyst
1958-64		discovery/commercialization of sedimentary zeolite deposits in western U.S. and Japan
1958	Mobil	zeolite synthesis with organic cations
1962-85	Mobil/Union Carbide	synthesis of high silica zeolites
1982	Union Carbide	synthesis of microporous $AlPO_4$ sieves
Recent Developments		
1985-94	Industries/Universities	synthesis of "large pore" (e.g., VPI-5, cloverite), and mesopore (MCM-41) materials

Today synthetic zeolites are the most important catalysts in petrochemical refineries. They catalyze the cracking of larger hydrocarbons into high octane gasoline, the alkylation of aromatics, and the dewaxing of diesel fuel. They also separate xylene isomers for the production of synthetic polymers. Gasoline yield increases resulting from zeolite technology have exceeded 10% during the last two decades with an estimated added product value of $15-20 billion per year.[3]

Over 300,000 metric tons of synthetic zeolites are sold annually to consumers in powdered laundry detergents as environmentally friendly replacements for harmful polyphosphates. Synthetic and natural zeolites find numerous applications including water treatment, radioactive waste storage, gas separation and purification, desiccation, soil improvers, and animal feed supplements where their ion exchange and sorption properties are exploited.[4] Natural zeolites are used for pet litter, animal feed supplements, fertilizer carriers, oil absorbents, odor control, aquaculture, horticultural applications, desiccants, gas absorbents, catalysts, and water purification, in decreasing order of consumption. Sales in 1994 were 35,200 tons.[5]

More recently there has been a growing interest in the applications of zeolitic materials for recognizing, discriminating, and organizing atoms, molecules and atomic clusters. Chiral molecules and polymers, small metal particles, and semiconductor clusters confined in zeolite pores and cages impart interesting electrical and optical properties that may be exploited in sensor, energy conversion, and other electronic technologies.

In the mid-1950s, the potential application of zeolites as heterogeneous catalysts was recognized by industrial scientists. At that time several refinery processes (including catalytic cracking) employed amorphous aluminosilicate catalysts. Catalytic cracking reduces the molecular weight of the heavier crude oil components by fragmentation to lighter molecules that comprise gasoline and other fuel products. It was an obvious step to evaluate synthetic aluminosilicate zeolites for catalytic applications, and in 1959 Union Carbide commercialized zeolite Y (synthetic faujasite with a higher Si/Al ratio than Zeolite X) for the isomerization of pentane and hexane.[6] However, the use of synthetic faujasites as cracking catalysts was hindered by their poor steam stability. This problem was solved by the ion-exchange of rare earth cations into the faujasite pore system.[7] The rare earth-exchange zeolite X exhibited excellent stability in the steam environments of the catalytic cracking and regeneration units. The commercialization of the faujasite-based Durabead 5 in 1962 by Mobil provided the refining industry with a catalyst that significantly outperformed amorphous aluminosilicates. The cracking activity of this new catalyst was over 1000 times that of the conventional amorphous aluminosilicate catalysts. Within several years of their introduction more than 90% of the catalytic cracking units in the United States were using faujasite-based cracking catalysts with significantly greater product yields. Zeolites also exhibited broad utility for catalyzing other organic reactions that proceed through carbonium ion intermediates, such as reforming, isomerization, and alkylation, which are all processes of commercial significance to the petroleum industry. The success of these catalytic applications assured a bright future for research on zeolitic materials.

The main properties of the zeolites in catalysis arise from:[8]

- the acidity of Brönsted or Lewis type sites
- the exchangeable cations (nature, location, accessibility of catalytically active cations)
- the metallic particles entrapped into the zeolitic cavities
- the size of the channel, openings and cavities, which regulates the diffusivity of reactants or products and the size of the intermediate reaction complexes, resulting in "shape selective" properties.

Syntheses with a variety of organic cations, resulted in a series of new high-silica zeolites including ZSM-5, ZSM-11, ZSM-12, ZSM-22, ZSM-23, ZSM-39, and ZSM-48. Several of these materials found applications in fuel and lubricant processing and chemical production. One of the most unusual applications was Mobil's methanol-to-gasoline (MTG) process.[9] Methanol, derived cheaply from methane in natural gas, is converted directly to high octane gasoline and water when passed over a ZSM-5 catalyst at reaction conditions.

The mineralogical community provides the basic definition of a zeolite:[10] A crystalline aluminosilicate with a 4-connected TO_4 (T = tetrahedral atom, e.g., Si, Al) tetrahedral framework structure bonded together via the oxygen atoms. Thus, the ratio of O/T is always equal to 2. An SiO_4 unit in a framework (structure) is neutral since an oxygen atom bridges two atoms and shares electron density with each (Figure 1-1). However, since Al is +3, for every aluminum containing tetrahedron there is a net -1 charge which must be balanced by a cation. The tetrahedra are coordinated such that the

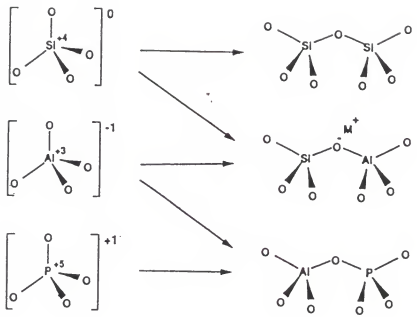

Figure 1-1. Basic building blocks of zeolites-molecular sieves.[10]

zeolites have open framework structures with high surface areas. Access to the cavities is possible through voids of various sizes which are of the size of small molecules.

Zeolites are usually represented with a general formula

$$M_xD_y(Al_{x+2y}Si_{n-(x+2y)}O_{2n})\cdot mH_2O$$

where M and D designate respectively a mono-(H^+, Na^+, K^+, Cs^+...) or a divalent (Ba^{2+}, Mg^{2+}, Ca^{2+}...) cation, which has considerable freedom of movement, permitting ion exchange and reversible dehydration. As with most definitions and classifications, there are usually borderline examples, and zeolites are no exception. Synthetic zeolitic materials include several examples that do not meet the mineralogical criteria. Microporous aluminophosphates and silicas have neutral frameworks with no charge-balancing cations.

The dimensional properties of some zeolites are reported in table 1-2. Depending on the tri- or mono- dimensional interconnections between cages, cavities or channels, the ease of transport of reagents and/or product molecules through the zeolitic network will vary. On the basis of pore size, zeolites can be classified in three groups: the large pore zeolites, which present twelve-membered rings (such as mordenite and faujasite), the intermediate pore zeolites with 10-membered rings (such as ZSM-5, ZSM-11, ferrierite) and the small pore zeolites with 8-membered rings (such as erionite, A, chabazite, ZK-5).

Sometimes, the size of the pores or cavities can be comparable to the critical molecular dimensions of some hydrocarbons.[11] Some examples are presented in Table 1-3.

Table 1-2. Size of Cavities and Pore Structure of Some Zeolites.

Zeolites	Type of Cavities	Number of Oxygens (ring openings)	Size of Channels (nm)
Chabazite	20-hedron	8	0.36x0.37
Erionite	23-hedron	8	0.36x 0.52
Faujasite (X,Y)	Sodalite	12	0.74
	supercage (26-hedron)		
Offretite	14-hedron	12	0.64
		8	0.36x0.52
Sodalite	Sodalite cage	12	0.74
ZSM-5	Pentasil	10	0.54x0.56
		10	0.51x0.55
Mordenite Z	Pentasil	12	0.64x0.70
		8	0.29x0.57
ZK-5	18-hedron	8	0.39
	26-hedron		

Table 1-3. Critical Molecular Sizes.

Molecules	Critical Diameter (nm)	Chain Length (nm)
n-paraffins		
C_2	0.47	0.53
C_3	0.47	0.65
C_4	0.47	0.78
C_6	0.47	1.03
C_{10}	0.47	1.53
iso-paraffins	0.54	
aromatics		
benzene	0.68	
toluene	0.68	
p-xylene	0.68	
o-, m-xylene	0.74	
1,3,5-trimethyl-benzene	0.84	
1,3,5-triethyl-benzene	0.92	
1,3,5-triisopropyl-benzene	0.94	

The synthesis of zeolites is complicated and the reactions are not well understood. The crystallization of these solids first involves the polymerization of silicate anions in the solution mixture. Polymerization depends on the pH, the OH^-/H_2O ratio, the reactant relative concentration, the stirring intensity, the temperature, etc. Usually synthesis occurs under elevated pressure. The synthesis conditions (concentrations of reactants, temperature, pH, duration of synthesis...) result in different sizes and morphologies of zeolitic grains and determine homogeneous versus heterogeneous Al distribution in the zeolitic framework and along the grains.[12] It follows that catalytic properties, particularly

shape selectivity, and aging by coking, are greatly influenced by such differences. For instance high Si/Al ratio and monomeric Na silicate in the mother solution result in small ZSM-5 microcrystallites while Al rich ingredients and polymeric silica yield large crystals. There is a competitive interaction between alkali and organic cations with the aluminosilicate polymeric anions. The structure-directing role of cations in zeolite synthesis has recently been reviewed by Barrer.[13] According to this work:

1) Na^+ in the reaction mixture favors the formation of sodalite and cancrinite hydrates, faujasites, and zeolite A;

2) K^+ favors the formation of chabazite and zeolite L;

3) Solutions containing Ca^{2+} favor the formation of thomsonite and epistilbite;

4) Sr^{2+} favors zeolites of the heulandite and ferrierite types;

5) Ba^{2+} and Li^+ ions favor different kinds of synthetic zeolite frameworks.

The use of organic cations has opened the field for the synthesis of new zeolites. These cations are thought to increase the solubility of the silicate and aluminate ions and to arrange the water molecules in a template-like fashion. Using tetramethylammonium cations, X and Y type zeolites were synthesized. Alkylammonium (R_4N^+), alkylphosphonium (R_4P^+) and other organic complexes were also used.[14] More recently the use of tetrapropylammonium and tetrabutylammonium cations resulted in the formation of new zeolites designated ZSM-5 and ZSM-11 respectively by Mobil.[15,16] Their interconnecting channels present a very interesting spatial configuration because of their structure (no cavities), the limited size of the channels (≈ 0.55 nm) and the three dimensional traffic of molecules. The limited size of the product hydrocarbons (C_n with $n < 10$) results in low

coking and deactivation rates in methanol conversion reactions. This is a characteristic of selective zeolites.

It was also observed that with different spatial configurations of channels, cavities, pores, etc, the catalytic properties are changed and the selectivity changes to less bulky molecules due to limitation in void volume near the active sites or to resistance to diffusivity. This feature, termed "shape-selectivity", was first proposed by McBain.[17] For example, selective cracking of linear paraffins was obtained from petroleum reformate streams resulting in an improvement of the octane number, which is known to be higher for branched paraffins and for aromatics than for linear paraffins. Shape selectivity usually combines acidic sites within the zeolite pore structure with the spatial arrangements and interconnection of the channels and cavities. Industrial applications of zeolites are summarized in Table 1-4.

There are several types of shape size selectivity in zeolites. First, the reactant molecules may be too large to enter the cavities. This kind of selectivity is called reactant shape selectivity and is illustrated in Figure 1-2.

Table 1-4. Main Commercial Processes Involving Zeolites.

Process	Catalyst	Benefit
Catalytic cracking	RE-Y, US-Y	high conversion rate
Hydrocracking	Co, Mo, W, Ni on faujasite, mordenite, erionite	high conversion rate
Toluene disproportionation	ZSM-5	increase in p-xylene yield
Alkylation of aromatics	ZSM-5	increase in p-xylene and ethyl-benzene yields. Low by-product formation
Xylene isomerization	ZSM-5	Increase in p-xylene yield. Low by-product yield.
Dewaxing	Ni/ZSM-5	Increase in octane number
Selectoforming	Ni/erionite	Increase in octane number LPG production
Methanol to gasoline	ZSM-5	High yield of gasoline with high octane number

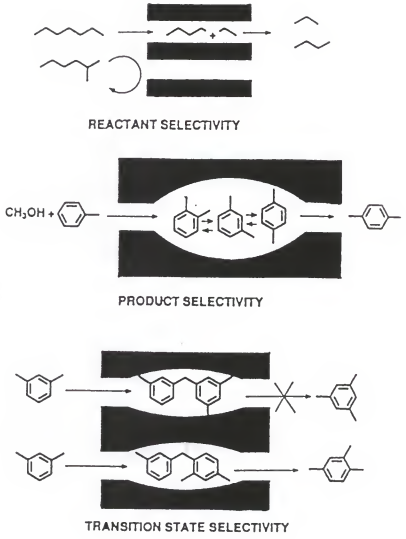

Figure 1-2. Representation of the types of shape selectivity exhibited by zeolites.[10]

Product shape selectivity occurs when reaction products of different sizes are formed within the interior of the zeolite crystals and some of the products formed are too bulky to diffuse out. The products which cannot escape from the cavities may undergo secondary reactions to form smaller molecules or may deactivate the catalyst by blocking the pores. A classic example of this type of selectivity is the monomolecular isomerization reactions of alkylaromatics[18] as depicted in Figure 1-2.

Another type of shape selectivity is transition-state selectivity. For this type of selectivity, certain types of transition-state intermediates are too large to be accommodated within the pores/cavities of the zeolites. However, neither the reactants or the products are restricted from diffusing through the pores of the zeolites. A good example of this type of selectivity is the transalkylation of dialkylbenzenes.[18]

The work presented in this dissertation is concerned with investigation of acidity of zeolites. A variety of techniques has been reported to measure acidity including the use of Hammett indicators,[19] measurement of adsorption and Temperature-Programmed Desorption of base molecules, dealkylation rates, isomerization and dehydration rates, IR spectroscopy and NMR of chemisorbed probes.[20]

Some of the more recent articles in this area have employed solid-gas calorimetric measurements to measure acidity and there are limited studies reporting calorimetric measurements of solid acids slurried in non-basic solvents.[21]

Considering that the acidity of a solid catalyst is manifested by the conversion of an adsorbed neutral base into its conjugated acid, the simplest and most widespread method of the acid strength estimation for a solid catalyst employs a suitable color

indicator adsorbed on its surface.[22] In order to apply this method it is assumed that the pH scale used to determine acid strength in dilute aqueous media can be extrapolated to very strong acid media by means of overlapping indicator comparison. By use of an appropriate series of indicators, the extrapolated pH scale is given by H_o, the Hammett acidity function.[19] When the indicator (B) reacts with a Brönsted acid (AH) to form the corresponding conjugated acid (HB^+) and base (A^-), the acid strength is expressed by the Hammett acidity function in the following way:

$$H_o = pK_a + \log [B]/[BH^+]$$

In the case of the interaction with a Lewis acid site, H_o is expressed by

$$H_o = pK_a + \log [B]/[AB]$$

where [B] is the concentration of the neutral base which reacted with the Lewis acid or electron pair acceptor, A.

At this point, the acid strength of a solid catalyst can be estimated by noting which members of a series of Hammett indicators are adsorbed in the acid form. If the color is that of the acid form of the indicator, then the value of the H_o function of the surface is the same or lower than the pK_a of the conjugated acid of the indicator. Then, the lower the pK_a of the color changing indicator is, the greater the acid strength of the solid. Indicators with different pK_a values and amine titration give the number of acid sites of various acid strengths.

Indication method suffers from a large number of limitations. Equilibrium is rarely achieved, and therefore acidity data from indicator methods can not be used to predict catalytic behavior. Moreover this method gives the sum of the amount of

Brönsted and Lewis acid sites. Another problem arises from the visual determination of the color change, which become even more subjective when colored or dark catalyst samples are used.

Another technique widely used for characterizing acidity in zeolites is Temperature-programmed desorption (TPD) of ammonia.[23] There are many variations in the method, but it typically involves saturation of the surface with ammonia under some set of adsorption conditions. Physically adsorbed ammonia is removed by prolonged evacuation and whatever is left on the surface is assumed to be chemically adsorbed. A linear ramping of the temperature of the sample follows in a flowing inert gas stream. Ammonia concentration in the effluent gas is determined by absorption/titration or mass spectroscopy. Alternatively, the experiment may be carried out on a microbalance and changes in sample mass may be followed continuously.

It is difficult to ensure that "physically adsorbed" species are not counted along with the ammonium ion sites. Desorption from nonprotonic binding sites can take place over a wide temperature range, even at temperatures approaching 600 K, where it is normally assumed that only Brönsted sites are adsorbing the NH_3.[24] This desorption is dependent on experimental conditions like sample bed depth, carrier gas dynamics, pore size and temperature control. Deconvoluting the desorption trace to obtain Brönsted site concentrations generally requires very careful experimental control and may not be possible under all conditions. In addition, it has to be considered that this procedure may be misleading if ammonia dissociates giving NH_2^- and H^+ species which would be adsorbed on both acid and basic sites. This type of dissociation depends on the kind of

solid and on the adsorption conditions. When the solid has two types of acid sites, e.g. Brönsted and Lewis sites , but only one is catalytically active, the TPD results will not correlate with catalytic activity, unless the adsorption on the two sites is differentiated by some other technique.[11] Finally, the determination of heats of desorption from ammonia TPD plots is not straightforward, and in spite of the large number of papers that purport to be able to extract acid strength distributions from desorption traces, the accumulated data show little consistency.

Drago has developed a calorimetric method based on enthalpies of interaction and adsorption isotherm measurements. This has become known as the cal-ad method.[25] The method involves slurrying a solid acid in a non-interacting solvent and measuring the heat of interaction between the solid acid and a known amount of injected basic probe. This heat is recorded by a thermistor and translated to an enthalpy using computer software. The adsorption part of the experiment is done to determine the extent of complexation of the base. The calorimetric technique has the advantage of being able to differentiate acid site strengths and the number of sites with a particular strength. Therefore, this method has been used as a tool to measure quantitatively the acidity of different zeolites. The advantage of this procedure is that it provides the equilibrium constant ($K_{ad,i}$), the enthalpy (ΔH_i) and the number of acid sites (n_i) for each of the i-different types of sites in the solid.

Many other analytical techniques are useful for characterizing solid acid catalysts, such as ICP, NAA, AAS, TGA, powder XRD, IR, ^{29}Si, ^{27}Al, ^{1}H NMR analysis. These techniques have also been used in our efforts to determine patterns of acidity in zeolites.

CHAPTER 2
INVESTIGATION OF ACIDITY OF HZSM-5

Introduction

ZSM-5 has been studied more than any other zeolitic material including several structure refinements. Interest in ZSM-5 has resulted from diverse catalytic applications including cracking, isomerization, dewaxing, methanol-to-gasoline conversion, and many others.[26] ZSM-5 was originally synthesized with tetrapropylammonium (TPA) templates. Subsequently it has been synthesized with different organic and inorganic molecules.[27]

The structure of ZSM-5 is difficult to describe and depict because of the large unit cell and a 3-dimensional pore system. The simplest description is from van Koningsveld et al.[28] The framework fragment (in bold) containing 12 T-sites (T = tetrahedral atom, e.g., Si, Al) in Figure 2-1(a) forms a chain along *c* by the application of a 2-fold screw axis parallel to *c*. Inversion centers produce additional chains and generate the (010) pentasil layer with 10-membered tetrahedral-atom rings, which define a linear channel parallel to [010]. Linking (010) pentasil layers with their mirror images completes the 3 dimensional framework and produces pentasil layers (Fig 2-1b), which also have ten atom rings that define another sinusoidal channel system parallel to [100]. The MFI

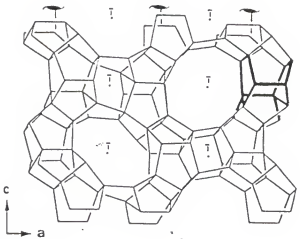

(a)

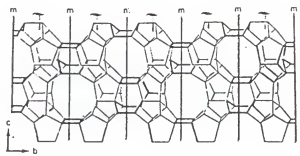

(b)

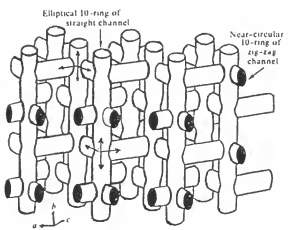

(c)

Figure 2-1. (a) Framework Topology and Symmetry Elements of the (010) Pentasil Layer in ZSM-5 (MFI). The 12T-atom Building Unit is shown by bold lines; (b) (100) Pentasil Layer in Pnma (As-synthesized or High Temperature) ZSM-5; (c) Representation of the Channel System in ZSM-5.

framework contains an intersecting, 3-dimensional, 10-ring pore system which is depicted schematically in Figure 2-1(c).

In spite of considerable effort, the measurement of acidity and understanding the role that acidity plays in the catalyzed chemical conversions remain key problems in the solid acid area.[29,30] Recent reports from this laboratory[25,31] have described a cal-ad procedure for evaluating the acidity of solids, which employs the combined measurements from adsorption and calorimetry studies to define the solid-base (or acid) equilibria better than is possible with the separate measurements. This procedure provides the equilibrium constant ($K_{ad,i}$), the enthalpy (ΔH_i) and the number of acid sites (n_i) for each of the i-different types of sites in the solid. The individual site contributions to the total heat are determined with the K values, so the assumption that only the strongest site is coordinated is not made. The resulting donor-acceptor enthalpies provide a scale of solid acidity that is temperature independent from room temperature up to temperatures where acid catalysts are commonly used (200 - 300 °C).

A fundamental acidity scale of solids will require a evaluation of the reaction involved. Solution acid-base equilibria, which are well understood, invariably involve displacement reactions. Even in alkane solvents, solvent molecules undergoing dispersion interactions with the acid and base are displaced when the donor coordinates to the acid. Earlier results from this laboratory[32] have shown that in poorly solvating solvents the product and reactant non-specific dispersion interactions cancel and do not contribute to measured enthalpies. In contrast, gas phase donor-acceptor interactions, e.g. proton and cation affinities, are not displacement reactions and have dispersion as well as

donor-acceptor contributions to the measured enthalpies. In contrast to solution enthalpies, that are fit to a two term electrostatic-covalent model, the quantitative correlation of gas phase ion-molecule reactions requires[32c,d] a transfer term to accommodate the electron transfer and dispersion components that are minor in solution displacement reactions. This transfer term is appreciable even for the proton affinity of argon ($E_B = C_B = 0$ for argon) in which case the transfer contribution is mainly a dispersion interaction. The very large dispersion and transfer terms make proton transfer a very poor model for condensed phase reactions and account in part for the poor correlation $R^2 = 0.79$ when gas-solid enthalpies of reactions of zeolites with substituted pyridines and amine[33] are plotted vs. proton affinities.

As a result of the above considerations, reactions of solid acids with bases in poorly solvating solvents will not produce the same enthalpy as measured in gas phase-solid reactions but can provide complimentary information with differences providing an estimate of the gas-solid dispersion component. One can argue that solution enthalpies devoid of dispersion contributions provide a better scale of acidity for solids. Even a gas phase, solid acid catalyzed reaction is a displacement reaction in which products are displaced by reactants. The dispersion component is partially canceled and donor-acceptor contributions dominate substrate binding. Furthermore, as manifested in spectral shifts, strong donor-acceptor interactions make much larger perturbations in the electronic structure of a molecule than dispersion interactions.[34] Acid catalysis occurs because of the changes induced in the electronic structure of the coordinated molecule.

Clearly understanding differences in the reactivity of zeolites, will require understanding differences in their donor-acceptor strengths.

This chapter will present the results from cal-ad studies aimed at measuring the acidity of HZSM-5. Studies with pyridine, 2,6-lutidine and 2,6-di-t-butylpyridine provide a unique thermodynamic characterization of the acid sites and their distribution in the solid. The factors that lead to an incorrect assessment of the acidity and number of strong acid sites with gas-solid calorimetry, TPD and isopropyl amine decomposition are discussed.

Experimental

Materials

HZSM-5 (Lot No. 91101036K), from the PQ corporation, with an advertised bulk Si/Al ratio of 30, 0.05% Na_2O and surface area of 430 m^2/g was used. Our atomic absorption measurements indicated that the bulk Si/Al ratio was 36. Infrared, calorimetric and adsorption studies were carried out on samples that were dried under flowing oxygen for two hours at 450 °C and then evacuated at 450 °C overnight. The oxygen flow was used to assure that no organic material was present in the samples. Elemental analyses were performed by the Microanalysis Laboratory at the University of Florida, and carbon as well as nitrogen was absent on the original and calcined samples. The drying apparatus was filled with argon and transferred to a dry box to load the calorimetric cell.

Pyridine (Fisher) was distilled over CaH_2 using a 12 in. Vigreux column. 2,6-di-tert-butylpyridine and 2,6-lutidine (Aldrich, 97 %) were used as supplied. Hexane (Aldrich, 99%) was distilled over P_2O_5 and stored over 4 Å molecular sieves.

Calorimetric Measurements

One gram samples of HZSM-5 were slurried in 100 ml of hexane and reacted with pyridine, 2,6-lutidine or 2,6-di-t-butylpyridine solutions in hexane. Addition of base solutions to the calorimeter were made using a 2.5 ml Hamilton gas-tight syringe with calibrated stops. The heat evolved was measured after each injection. The calorimeter is a 150 ml silvered dewar flask equipped with a heater coil and thermistor (Figure 2-2). The thermistor is calibrated prior to each calorimetric experiment. Repeat calorimetric runs gave an average deviation of 0.005 calories.

Adsorption Measurements

Adsorption experiments were carried out using one gram of HZSM-5 in a sealed round bottom flask containing 100 ml of hexane (Figure2-3). After each injection, at least three minutes were allowed for equilibrium to be reached. Then a 1 ml sample is removed from the flask and placed into a quartz 1 cm uv-vis cell. One ml of solvent is added back into the flask to maintain a constant volume. The singular absorbance of pyridine at 251 nm, 2,6-di-t-butylpyridine at 258 nm, and 2,6-lutidine at 265 nm is measured with a Perkin Elmer Lambda 6 UV/VIS spectrophotometer and these

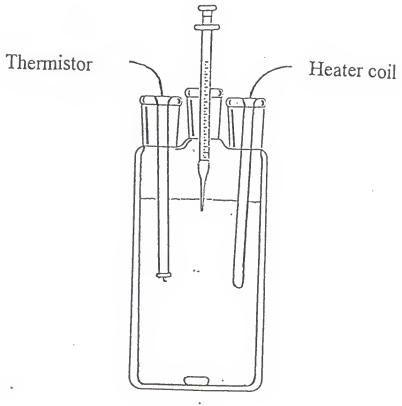

Figure 2-2. Calorimetric Aparattus.

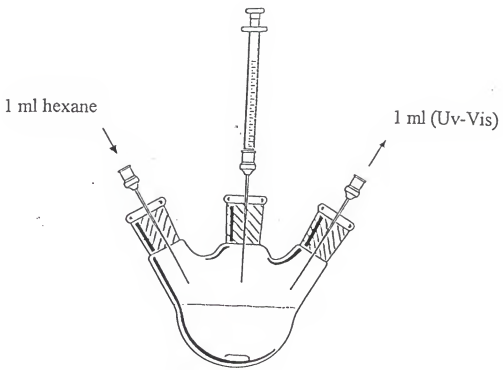

Figure 2-3. Adsorption Aparattus.

absorbances are used to calculate the concentrations of pyridine, 2,6-lutidine and 2,6-di-t-butylpyridine in solution at equilibrium. By knowing both the amount in solution at equilibrium and the amount added, the amount absorbed by the solid is given by the difference. Since one is combining raw data from calorimetric and adsorption measurements in the data analysis, it is essential in the cal-ad procedure to use the same ratio of solid to solution in both measurements. Repeat titrations give absorbance values with an average deviation of 0.003 absorbance units.

Cal-ad Analysis

It is important that the concentration of base and the ratio V/g where, V is the volume of solution (liter) and g is the mass of solid (grams), be the same in both the calorimetric and adsorption experiments. Since we need to resolve site 1 and site 2 contributions to $-\Delta H_{AVE}$, it is important to use very dilute solutions of pyridine in the titration. It is also important to add eventually a total amount of pyridine that will saturate at least 60% of site 2. Since porosity can lead to a large K for binding even when $-\Delta H$ is small, the usual cal-ad procedure of fitting the adsorption data first to generate concentrations of base in solution for the subsequent fit of the heat evolved cannot be used. In the case of HZSM-5, for example, detectable amounts of pyridine are not seen in solution until 0.1 mmol of pyridine has been added (Point 7 of increasing concentration in Figure 2-5). Accordingly, the data work up differs slightly from that reported for silica gel.[31] By entering the equilibrium concentration of pyridine in solution calculated from the adsorption experiment into the calorimetric expression, rough estimates of n's and

K's are obtained for site 1 and site 2. The following equation is used to produce these first estimates:

$$\frac{h}{g} = \sum \frac{n_i K_i [B]}{1 + K_i [B]} \Delta H_i$$

where:

h is the sum of heat evolved from calorimetric experiment = Σ ([T] - [B]).v.ΔH_i,

ΔH_i is the enthalpy for binding to each site,

[T] is the total concentration of base added (mol/l) in each injection from calorimetric experiment, and

[B] is the equilibrium concentration of base in solution.

The resulting K's and n's are used to generate an adsorption isotherm from which the equilibrium concentrations of base in those solutions that are too small to measure are calculated for each point in the adsorption curve. Rather than graphically interpolate the adsorption isotherm to obtain these concentrations, the isotherm is fit to a polynomial series.

For one site the following series is used:

$$(v / g)[T] = x^1 [B]^2 + x[B]$$

where,

v/g = volume (liters)/mass of solid (grams),

$[T]$ is the total concentration of base added (mol/l) for each injection in the calorimetric experiment,

$[B]$ is the equilibrium concentration of base in solution,

$x^2 = v/g.K_1$ and $x = n_1.K_1 - v/g.K_1.[T] + v/g$

For two sites the following series is used:

$$(v / g)[T] = x^3[B]^3 + x^2[B]^2 + x[B]$$

where,

$x^3 = K_1.K_2.v/g$; $x^2 = n_1.K_1.K_2 + n_2.K_1.K_2 - v/g.K_1.K_2.[T] + v/g.K_1 + v/g.K_2$; and

$x = n_1.K_1 + n_2.K_2 - v/g.K_1.[T] - v/g.K_2.[T] + v/g$

These concentrations are then used as the experimental base concentrations in solution for the adsorption isotherm for those solutions too dilute to measure and the combined adsorption and calorimetric data are solved for the best fit n's and K's . These n's and K's are then used in the above expressions to recalculate the concentrations of base in solution for those systems too dilute to measure as described above and the combined adsorption and calorimetric data refit. This procedure is repeated until the K's and n's converge. This procedure differs from that utilized for silica gel and is recommended for porous solids that have such large affinities for adsorbates that solution concentrations cannot be determined even when $-\Delta H$ is small.

Infrared Measurements

All IR spectra were recorded as Nujol mulls on sodium chloride plates, using a Nicolet 5DXB FTIR spectrophotometer.

Solid-State NMR

Solid-state ^{1}H, ^{27}Al and ^{29}Si NMR spectra were recorded under magic angle spinning (MAS) at room temperature on a Bruker MSL-300 spectrometer at 300.13, 78.15, and 59.62 MH_z, respectively. The rotors were driven by dry air, and the magic angle was set precisely by observing the ^{79}Br resonance of KBr. All the spectra were recorded with a 4 mm MAS probe.

Prior to ^{1}H MAS NMR experiments, the sample was dehydrated in 10 mm o.d. glass tube for 6h at 673 °K under vacuum (pressure of 10^{-5} mbar) and transferred under controlled atmosphere into the rotor. No rehydration occurred during the experiments as shown by ^{1}H NMR. The spectrum was recorded following an echo sequence ($\pi/2$-τ-π) where the echo time τ is equal to the inverse of the spin rate, $\pi/2$ is 5μs and the pulse delay is fixed to 30s (full relaxation). The chemical shift is referenced to external tetramethylsilane. The rotor was spun at a rotation frequency of 10 KHz. For ^{29}Si, one pulse sequence with a $\pi/2$ pulse of 5μs was used. The cycle time of 60s gives complete relaxation of the spins of the silicon species. The ^{27}Al spectrum was recorded using a one pulse sequence with a $\pi/8$ pulse i.e. 0.6μs and high power proton decoupling. A $\pi/2$, 5μs pulse was used for the liquid reference. The rotors were spun at 10KHz. The shifts are referenced to external TMS and aqueous hexaquo aluminum nitrate respectively.

The amount of each silicon environment per unit cell can be calculated with the following equations:[35]

$$[Si / Al]_{Framework} = \frac{\sum_{n=0}^{4} Si(nAl)}{0.25 \sum_{n=0}^{4} nSi(nAl)} = \frac{Si(1Al) + Si(0Al,1OH) + Si(0Al)}{0.25Si(1Al)}$$

The last term results because only n = 0 and n = 1 species are present at this low aluminum content.

The spectra were deconvoluted using the WINFIT 950425 program from Bruker GMBH.

Results and Discussion

In view of confusing terminology in the zeolite literature, it is important to define the terms used in the donor-acceptor literature and in this article. The term Lewis acid will be reserved to distinguish aluminum or silicon atom acceptor centers. There is no evidence for this type of site in HZSM-5 from our work. The terms Brönsted site and hydrogen bond site are used to distinguish the products of a reaction. Any protonic site is a potential Brönsted site if a strong enough base is employed. A site that hydrogen bonds to pyridine without proton transfer will not transfer the proton to most neutral organic bases and will be called a hydrogen bond site. Sites that proton transfer to pyridine will be called a Brönsted site but could function as a strong hydrogen bond site toward a weak donor.

Infrared and NMR studies of HZSM-5

HZSM-5 was chosen as the first zeolite to be studied by cal-ad in view of the extensive characterization reported for this material. Zeolites have high affinity for water and precautions must be taken to dry the samples well and to exclude water during the measurements. Figure 2-4 shows the infrared spectra in the hydroxyl region of the sample as received and that after drying for 24 hours at 450 °C under vacuum with periodic flushing of the apparatus with argon. After drying, two bands remain: a sharp one at 3694 cm^{-1} and a broad band at 3457 cm^{-1}. The latter is attributed to the bridging Al-(OH)-Si sites and the former to the nested silanols needed for charge compensation at a cation vacancy.[36] When the sample is deuterated and dried[36b] these two bands shift to 2750 and 2650 cm^{-1}. When this sample is titrated with pyridine in a calorimetric run, the spectrum of the remaining sample shows no adsorption in this region but has three bands in the pyridine region from 1624 to 1450 cm^{-1} that have been assigned to either Brönsted (pyridinium at 1543 and 1491 cm^{-1}) or hydrogen bond sites (pyridine adducts at 1624 cm^{-1}), as shown in Figure2-5. The absence of vibrations in the OH stretch region indicate water has been completely removed for a pyridine-H_2O adduct would absorb in this region. The ^{1}H, ^{27}Al and ^{29}Si solid state NMR in Figure 2-6 (a-c) (vide infra) also confirms the absence of water.[35] All reported calorimetric results are for dried samples of HZSM-5 that were checked by infrared to ascertain the absence of water. In view of the difficulties associated with obtaining information about acidity from the fine structure of infrared OH bands[37, 38] no further analysis of the infrared spectra were undertaken.

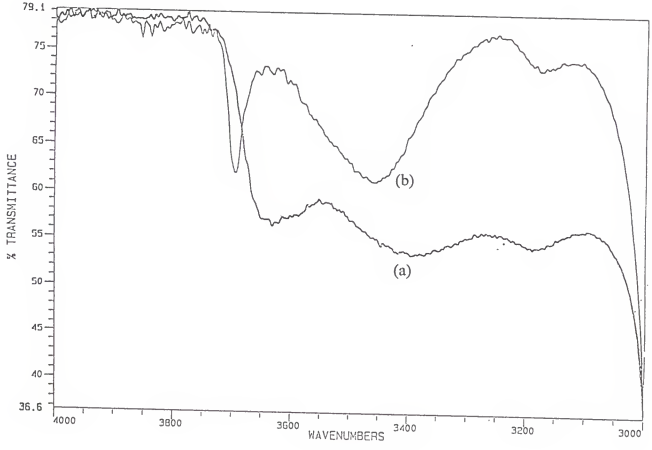

Figure 2-4. FTIR Spectra in Nujol Mulls of HZSM-5 (a) as Received and (b) After Drying at 450 °C in Vacuum.

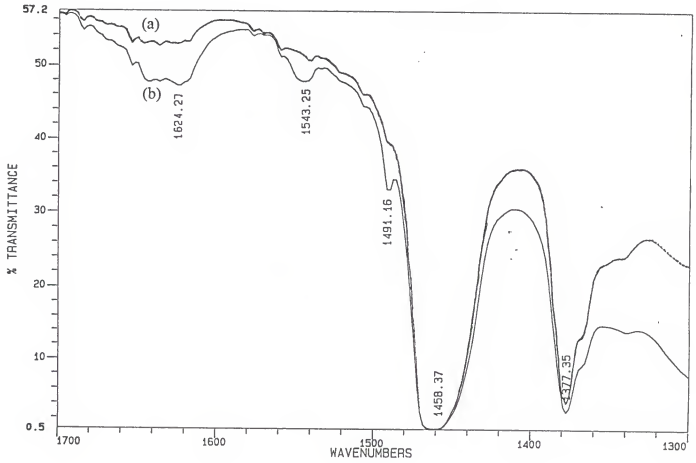

Figure 2-5. FTIR Spectra in Nujol Mulls of HZSM-5 (a) Dried and (b) After Calorimetric Titration with Pyridine.

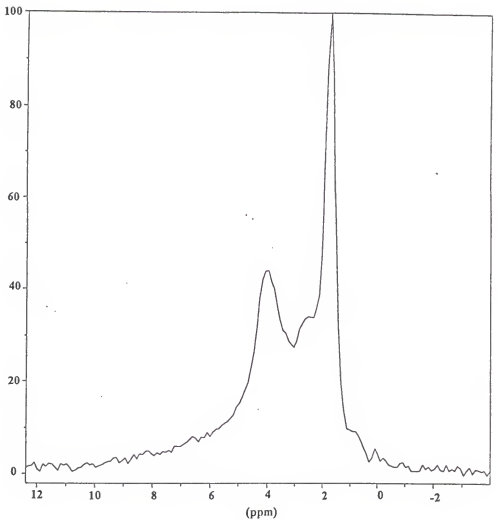

Figure 2-6 (a). ^{1}H NMR Spectrum of Solid HZSM-5. $\delta = 4.0$ ppm (bridging hydroxyl AlOH), $\delta = 2.5$ ppm (extra-framework AlOH) and $\delta = 1.7$ ppm (silanol groups SiOH).

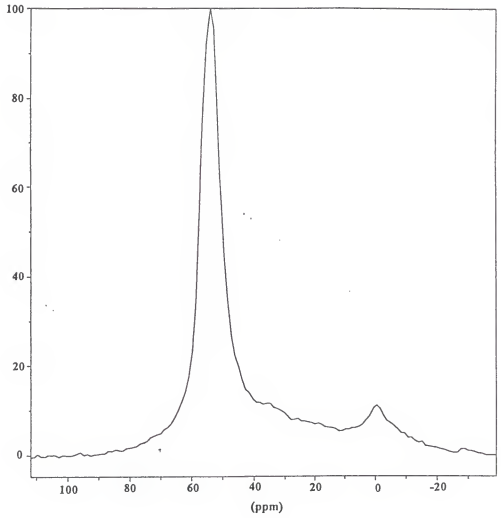

Figure 2-6 (b). ^{27}Al NMR Spectrum of Solid HZSM-5. δ = 54 ppm (tetra-coordinated framework Al), δ = 0 ppm (hexa-coordinated extra-framework Al).

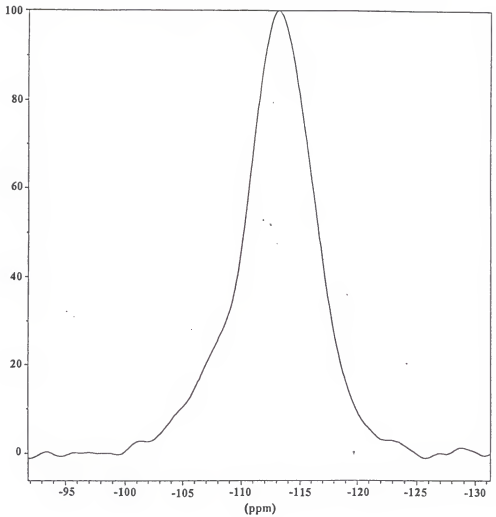

Figure 2-6 (c). ^{29}Si NMR Spectrum of Solid HZSM-5. δ = 117.0 and 113.2 ppm (non-equivalent Si atoms bonded to other Si).

Limitations in Average Enthalpies from Calorimetry

Cal-ad results for HZSM-5, particularly the quantity of sites, are expected to be sample dependent. Thus it is important to emphasize that the results reported here are for a sample with a bulk Si/Al ratio of 36 and with the spectral features described above and in the NMR section. A material used commercially in catalytic reactions is selected for study. The base pyridine is selected as the donor in order to avoid the amphoteric interaction encountered when protonic donors (e.g. NH_3) are studied. When NH_3, RNH_2 and R_2NH are employed,[39,33] electron pair donation by the donor makes the N-H proton more acidic which can lead to increased hydrogen bonding of this N-H proton to the framework. This secondary hydrogen bonding by the N-H proton is analogous to the interactions of zeolites with water.[37b] Upon coordination of water to the Brönsted or hydrogen bond site of the zeolite, a secondary hydrogen bonding interaction of a water O-H to the oxygen of an Si-O-Si group occurs. With protonic bases, amphoteric hydrogen bonding interactions would give added contributions to the measured enthalpies and distort the solid acidity data.

The adsorption and calorimetric measurements of pyridine, 2,6-lutidine, and 2,6-di-tert-butylpyridine by HZSM-5 are shown in Figures 2-7, 2-8 and 2-9, respectively, where the millimoles of base adsorbed by one gram of the solid slurried in 100 ml of hexane are plotted vs the amount of base in solution. The h' axis of Figures 2-7, 2-8 and 2-9 is a plot of the heat evolved when the bases are added to one gram of HZSM-5 slurried in 100 ml of hexane.

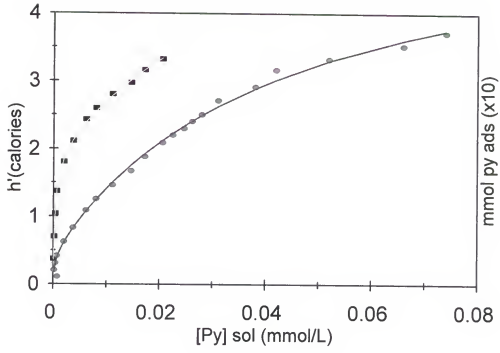

Figure 2-7. Adsorption isotherm and heat of adsorption versus concentration of pyridine in solution: (■) calorimetric points, (●) adsorption data points, and (—) solid line: calculated using values from Table 2-2.

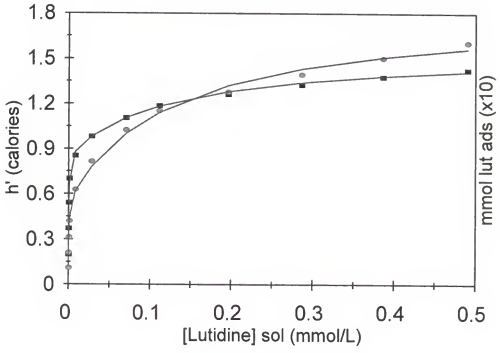

Figure 2-8. Adsorption isotherm and heat of adsorption versus concentration of 2,6-lutidine in solution: (■) calorimetric points, (●) adsorption data points, and (—) solid line: calculated using values from Table 2-2.

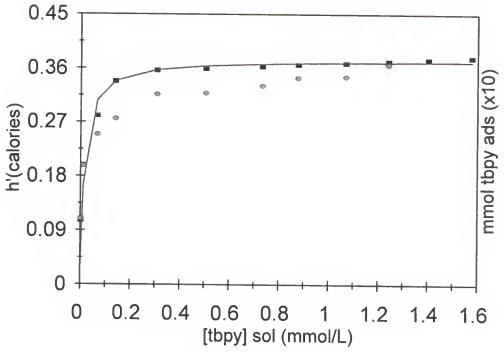

Figure 2-9. Adsorption isotherm and heat of adsorption versus concentration of 2,6-di-tert-butylpyridine in solution: (■) calorimetric points, (●) adsorption data points, and (—) solid line: calculated using values from Table 2-2.

Figure 2-10 is a plot of the average enthalpy of reaction calculated for those base additions in which 95% of the added respective base is adsorbed by the solid. Average data from the three titrations with 0.1 M base solutions are shown. The average enthalpy is calculated using a limited reagent assumption by dividing h' by the moles of base added and as such is an average of the sites that react with each incremental addition of base. This average enthalpy curve is easily calculated but it measures the enthalpy and amounts of the strongest sites only when a single type of site exists or when the equilibrium constants for different sites are significantly different ($\sim 10^3$). Since nearly all the pyridine is adsorbed even for those points where the $-\Delta H_{AVE}$ has decreased by a considerable amount, K_1 and K_2 are both large. The gradual decrease in $-\Delta H_{AVE}$, in contrast to a sharp break , indicates that the second site begins to react before the first site is completely reacted. The $-\Delta H_{AVE}$ decreases as weaker sites make a larger contribution to the average enthalpy. The essential question is: are there contributions to the $-\Delta H_{AVE}$ calculated for the first three base additions from a weaker site? This would make the enthalpy of site 1 larger than that given by $-\Delta H_{AVE}$ from the initial base additions. This question cannot be answered using only calorimetric data and introduces uncertainty in acidities reported in all the calorimetric literature studies[39,33,40] that calculate an enthalpy for a solid with multiple acid sites using the limiting reagent assumption.

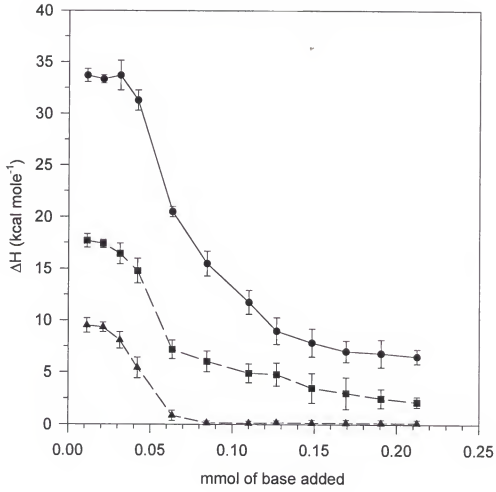

Figure 2-10. Average enthalpies of reactions versus mmol of base added.
● pyridine, ■ 2,6-lutidine, ▲ 2,6-di-tert-butylpyridine

The potential severity of the limiting reagent problem is illustrated with the data in Table 2-1. The table presents a hypothetical illustration of the moles of pyridine adsorbed on two sites for various K_2 and n_2 values when K_1 and n_1 are from cal-ad for our HZSM-5 sample; i.e., a K_1 value of 2×10^6 l/mol and an n_1 of 0.06 millimoles (Table 2-2).

Table 2-1. Hypothetical Illustration of Moles Adsorbed at Two Competing Sites as a Function of K and n.

Base	Moles Ads[a]	Moles Ads Site 2 ($\times 10^3$)				
Solution	Site1($\times 10^3$)	I[b]	II[c]	III[d]	IV[e]	V[f]
[M] ($\times 10^7$)						
1.17	0.0114	0.0007	0.0012	0.0023	0.0002	0.007
2.67	0.0209	0.0016	0.0027	0.0053	0.0005	0.016
5.01	0.0300	0.003	0.005	0.010	0.001	0.029
8.70	0.0381	0.005	0.009	0.017	0.002	0.048

a. $K_1 = 2 \times 10^6$ L/mol; $n_1 = 6 \times 10^{-5}$ moles/g
b. $K_2 = 1 \times 10^4$ L/mol; $n_2 = 6 \times 10^{-4}$ moles/g
c. $K_2 = 1 \times 10^4$ L/mol; $n_2 = 1 \times 10^{-3}$ moles/g
d. $K_2 = 1 \times 10^4$ L/mol; $n_2 = 2 \times 10^{-3}$ moles/g
e. $K_2 = 1 \times 10^3$ L/mol; $n_2 = 2 \times 10^{-3}$ moles/g
f. $K_2 = 1 \times 10^5$ L/mol; $n_2 = 6 \times 10^{-4}$ moles/g

The data are presented for the very low equilibrium base concentrations in solution that correspond to the first four base additions of the titration in Figure 2-10 for pyridine. For case I, when K_2 is 1 x 10^4 and n_2 is 0.6, the first base addition (0.01 millimoles/g) involves reaction of 6 % of site 2 and 94 % of site 1. By the fourth base addition, corresponding to 0.04 total millimoles of pyridine adsorbed per gram of zeolite, there is only 8.7 x 10^{-7} moles of pyridine in solution, and the values calculated for site 1 and 2 show that 13 % of the total base added coordinates to site 2. For the case in column II where K_1, n_1, and K_2 are the same as in case I, but n_2 is increased to 1.0 millimoles g^{-1}, the % of added base coordinated to site 2 in the first base additions increases from 6% to 11% and from 13% to 24% for the fourth base addition. Increasing n_2 to 2.0 (column III) results in 20 % of the added base coordinating to site 2 for the first base addition and 45 % coordinating to site 2 for the fourth addition. Values for other K's and n's are given in Table 2-1.

Clearly, one cannot compare the acidity of solid zeolites using an average enthalpy from a limiting reagent assumption unless K_1 is three orders of magnitude larger than K_2 and n_2 is less than two orders of magnitude larger than n_1. Since this information is not known, a priori, the K's and n's from gas phase calorimetric studies reported to date can not be trusted as a measure of strongest site strength.

Cal-ad Results

In contrast to studies based on the limiting reagent assumption, the cal-ad procedure simultaneously solves calorimetric and adsorption data (Figures 2-7, 2-8, and 2-9) to produce individual K's, -ΔH's, and n's for all the sites reacting with the bases. The solvent n-hexane was selected because it has a kinetic diameter around 4.3 Å.[41] Since the experimental data over the concentration range employed is fit to within experimental error of the measurement using a two-site model for pyridine and 2,6-lutidine, this number of sites is discriminated. The resulting thermodynamic values are given in Table 2-2. The accuracy of the site 1 equilibrium constants and entropies may be less than their precisions because nearly complete adsorption of base occurs up to the saturation point. The main conclusions will be drawn from enthalpies. The enthalpies for pyridine of donor-acceptor binding are -42.1 ± 0.8 and -8.6 ± 3.8 kcal $mole^{-1}$ for the two sites. Our studies extend up to 0.4 millimoles of pyridine added for 0.6 millimoles of total acid sites. Higher concentrations would improve the error limits of the site 2 parameters and might reveal that site 2 consists of two sites. However, our main concern is with site 1 parameters and these are defined well enough to produce accurate enthalpy values and quantities of the strongest site.

Table 2-2. Thermodynamic Parameters Obtained in Hexane Solvent for Reactions of HZSM-5 (Bulk Si/Al of 36) with Pyridine, 2,6-Lutidine and 2,6-di-t-butylpyridine.

	Pyridine	2,6-Lutidine	2,6-di-t-butylpyridine
n_1 (mmol/g)	0.0415 ± 0.0057	0.0529 ± 0.0074	0.0342 ± 0.0007
K_1^{298} (M^{-1})	$4.9x10^6 \pm 2.3x10^6$	$7.4x10^5 \pm 2.6x10^5$	$6.9x10^4 \pm 1.0x10^4$
$-\Delta H_1$ (kcal/mole)	42.1 ± 0.8	19.0 ± 0.3	10.9 ± 0.1
$-\Delta G_1^{298}$ (kcal/mole)	9.12 ± 0.3	8.00 ± 0.2	6.59 ± 0.1
ΔS_1 (cal/deg.mole)	-111 ± 2.8	-37 ± 1.2	-14 ± 0.4
n_2 (mmol/g)	0.53 ± 0.01	0.13 ± 0.06	
K_2^{298} (M^{-1})	$2.3x10^4 \pm 2.0x10^3$	$8.8x10^3 \pm 2.3x10^3$	
$-\Delta H_2$ (kcal/mole)	8.6 ± 3.8	5.4 ± 1.7	
$-\Delta G_2^{298}$ (kcal/mole)	5.95 ± 0.1	5.38 ± 0.2	
ΔS_2 (cal/deg.mole)	-9 ± 12.7	-0.1 ± 5.7	

Comparison of the enthalpy of interaction of pyridine for the first site with the enthalpy of reaction of pyridine with $SGAlCl_2$ (-51 kcal $mole^{-1}$) shows that HZSM-5 is not a superacid but is a considerably stronger acid than the strongest sites on silica gel (-12 kcal $mole^{-1}$) or γ-alumina (~ -18 kcal $mole^{-1}$). The thermodynamic data for the second site on HZSM-5 is comparable to that of the sites on silica gel. The equilibrium constants for pyridine reacting with silica gel and the second site of HZSM-5 are also of the same order of magnitude. In silica gel, these are not Brönsted sites toward pyridine. The infrared of adsorbed pyridine on silica gel indicates that the -12 kcal $mole^{-1}$ sites correspond to silanol hydrogen bonding sites ambiguously referred to as Lewis sites in the literature. Thus, site 2 in HZSM-5 is a hydrogen bonding site arising from bridging Al(OH)Si and SiOH functionality. The observation of a Brönsted peak in the infrared for adsorbed pyridine is attributed to site 1.

HZSM-5 contains 12 inequivalent T-sites. The excellent fit of the experimental data at low base concentration to this two site model indicates that the strong acid sites and the hydrogen bonding sites are homogeneous groups within the experimental resolution of our measurements (~ 2 kcal $mole^{-1}$). It is not possible to determine which of the different crystallographic sites in HZSM-5 have comparable acidities and are contained in the K_1 and n_1 values. Titrations with 2,6-lutidine and 2,6-di-tert-butylpyridine and ^{1}H, ^{29}Si and ^{27}Al NMR provide more information on this point (*vide infra*).

The line connecting the experimental h' values in Figure 2-11 gives the sum of the heat evolved for incremental additions of pyridine to one gram of HZSM-5 in hexane.

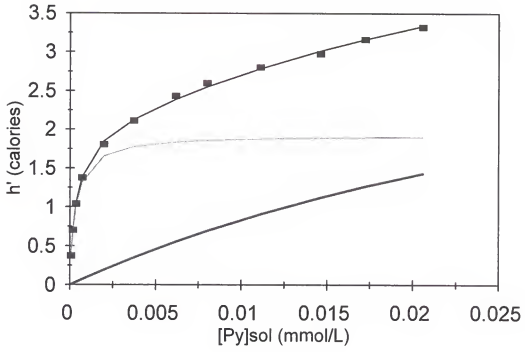

Figure 2-11. Sum of heat evolved versus concentration of pyridine in solution for two acid sites: (■) calorimetric data points, (--) dashed line: process 1 (first site), bold line: process 2 (second site), and (■) solid line: calculated using values from Table 2-2.

Using the data in Table 2-2, the experimental curve can be decomposed into the two contributions from sites 1 and 2. Site 1 (dashed line) reacts to completion in the titration. The second site (bold line) does not react completely. The contribution of the second site to all measured h' values, as calculated in Table 2-1, can be seen in this plot.

Figure 2-12 shows a similar plot of the contributions of the two sites to the adsorption data. The complete coordination of the strongest site is again seen (dashed line). Even though the adsorption data was measured in a concentrated pyridine solution, the second site is still incompletely coordinated by pyridine. Considering the error in n_2, 60-75 % of the second site has reacted at the highest concentration used.

Strong Acid Site Location

Cal-ad studies of the bases 2,6-di-t-butylpyridine and 2,6-lutidine help to elucidate the acidity of HZSM-5. These donors were selected because the former is too large to enter into the pores of HZSM-5 and access to the pores by the latter is expected to be limited. HZSM-5 is known to have two intersecting channel systems: one is straight and the other is sinusoidal and perpendicular to the former. Both channel systems have 10-membered-ring, elliptical openings with a 5.5 Å internal diameter. Saito and Foley[42] report two steps in the adsorption isotherms of high Si/Al ratio zeolites. The first peak in a pore size analysis corresponds to adsorption in pores of 5.5 Å diameter. The second peak, corresponding to a 7.7 Å diameter, does not correspond to a structural feature of the zeolite and is reported to be a non-physical result.

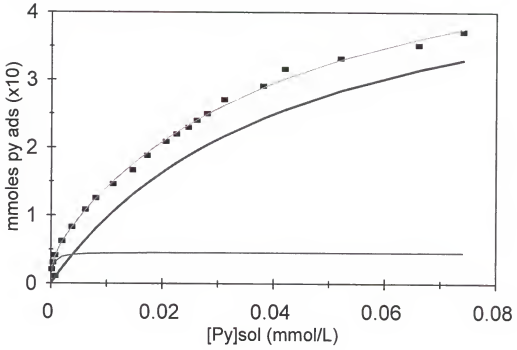

Figure 2-12. Adsorption isotherm versus concentration of pyridine in solution: (■) adsorption data points, (--) dashed line: process 1 (first site), bold line: process 2 (second site), and (■) solid line: calculated using values from Table 2-2.

Since 2,6-di-t-butylpyridine can not enter into the channels of HZSM-5, this titration gives information about the acidity of the external solid surface. The experimental data are fit to within experimental error of the measurement using a one-site model giving the values in Table 2-2. A considerably smaller enthalpy of -10.9 ± 0.1 kcal $mole^{-1}$ results compared to -42.1 kcal $mole^{-1}$ for pyridine. No strong acid sites are located on the exterior surface of the zeolite. The small n_1 value from this titration shows that the surface contains about 6 % of the weak n_2 type sites found for pyridine reacting with HZSM-5 with 94% of the acid sites being located in the channels.

The reaction of HZSM-5 with 2,6-lutidine produces a very interesting result. An enthalpy of -19 ± 0.3 kcal $mole^{-1}$ is obtained for the first site and an enthalpy of -5.4 ± 1.7 kcal $mole^{-1}$ for the second site. Site 1 for the donor 2,6-lutidine is not accessing the strong site 1 of pyridine. The low enthalpy for site 1 with 2,6-lutidine indicates that the strongest sites for this base are hydrogen bond sites. These enthalpies suggest site 2 for pyridine has large error limits because it contains the two sites detected with 2.6-lutidine.

The n-values are very informative. They suggest that the strongest sites for pyridine (-42 kcal $mole^{-1}$) and 66% of site 2 for pyridine are not accessed by 2,6-lutidine. Comparing n_1 for 2,6-lutidine and 2,6-di-t-butylpyridine indicates that there are 0.15 millimoles/g of hydrogen bond sites accessed by the former in addition to the 0.03 millimoles/g of surface sites. The second site for 2,6-lutidine like that for pyridine is very weak and could involve hydrogen bonding to isolated silanols at locations not accessed by 2,6-di-t-butylpyridine. Many of these sites are accessed by pyridine ($n_2 = 0.53$) and not by 2,6-lutidine ($n_1 + n_2 = 0.18$). The lutidine site 1 is tentatively assigned to arise

from the group of sites included in site 2 for pyridine. Studies at much higher concentrations of pyridine than those used in this titration are needed to discriminate the pyridine site 2 components.

The results from this study indicate a limited access strong site, I, limited access hydrogen bonding sites, II, interior hydrogen bonding sites III, and surface sites IV. Two types of intersecting channels exist in HZSM-5, one is straight and the other zig-zag. The latter contains crevases and curves that could contain the limited access strong Brönsted sites (I) and the hydrogen bond sites that cannot be accessed by 2,6-lutidine (II). The entropy for site 1 bonding to pyridine would suggest organization of the solid to accommodate the conjugate base.

Comparison of Cal-Ad with Other Acidity Measures

Much has been published on the acidity of HZSM-5 often leading to apparently conflicting conclusions which differ from those given above. In this section, we shall reinterpret results from reported indirect measures of zeolite acidity in order to show that the cal-ad measure of K, n and $-\Delta H$ is not inconsistent with any of these experimental observations.

HZSM-5 has been extensively studied by gas-solid calorimetry. At the elevated temperatures (~200°C) used in gas-solid microcalorimetry, the larger $-\Delta H$ and negative entropy change expected for site 1 than 2 lead to values of K_1 and K_2 that are much closer than those at room temperature. This leads to the expectation of simultaneous reaction of both sites of HZSM-5 with pyridine in the gas phase calorimetric titration producing a

constant $-\Delta H$ of 48 kcal mole^{-1} for up to 0.6 millimoles of added pyridine. The 0.6 millimoles correspond to the sum of n_1 and n_2 from the solution analysis supporting the prediction that the K's would be close and that both sites would react simultaneously producing an average enthalpy.

The larger $-\Delta H_{AVE}$ from the gas phase study compared to the cal-ad average is due to contributions from the dispersion component in addition to the donor-acceptor component to both sites 1 and 2 in the gas phase calorimetric study. Estimating the total gas phase enthalpies for site 1 and 2 at -75 and -43 kcal mole^{-1} for the purposes of illustration, a set of K's and n's could be found that after the first base addition caused reaction of site 1 and site 2 to occur in a ratio of 1:5 up to the 0.6 mmoles of base added. This would give a nearly constant $-\Delta H$ of 48 kcal mole^{-1} until site 1 was consumed. As more base is added the average enthalpy would then be dominated by the equilibrium involving site 2 until it is consumed. The purpose in proposing this scenario is to demonstrate that this or other combinations of $-\Delta H$'s, n's and K's cannot be eliminated when only calorimetry data is available. The results are ambiguous unless accompanied by a determination of K.

It would be of interest to factor out the dispersion and donor-acceptor components from gas phase calorimetric studies. Unfortunately, the reported gas phase values are some weighted average of sites 1 and sites 2. Temperature dependent studies[43] of the adsorption of gaseous propane by HZSM-5 give an enthalpy of -9.6 kcal mole^{-1}. Using a reported correlation[43], a value of about -22 kcal mole^{-1} is estimated for hexane using the van der Waals constant[43] and a similar value is expected for pyridine. This dispersion

component combined with the donor-acceptor component from cal-ad (-42 kcal $mole^{-1}$) leads to an expected gas phase enthalpy value of -64 kcal $mole^{-1}$ for pyridine reacting with the strong sites. The average enthalpy of -48 kcal $mole^{-1}$ reported from the gas phase calorimetric study is lower than -64 kcal $mole^{-1}$ consistent with the proposal that contributions from the second site are averaged in giving a low $-\Delta H_{AVE}$. It is interesting to note that the first few micromoles of pyridine corresponding to the first point in the gas-solid calorimetric titration of HZSM-5 give[39c] enthalpies of ~ -57 kcal mol^{-1}.

By using the procedures reported in our multiple equilibrium analysis of porous solids[43], it may be possible to resolve sites 1 and 2, by carrying out gas phase calorimetric measurements over a series of temperatures. Each new temperature introduces new K's but the -ΔH and n's remain constant so the added enthalpy data will help define K.

Consistent with the above discussion, the similarity in K's for the different sites at high temperatures also prevent TPD, TGA and DSC from resolving separate sites that differ substantially in strength, i.e., enthalpies. This adds to other reported complications involved in the use of these methods[44].

An infrared study[45] of HZSM-5 (Si/Al ratio of 47) in the –OH stretching region with and without adsorbed aromatics showed a heterogeneity of the OH functionality. Variations in the Si-O and Al-O distances, the Si-O-Al bond angles as well as the immediate environment in the channel contribute to the differences in the acid strength of the sites. Spectral deconvolution gives five sites, compared to the three found by cal-ad titration with pyridine, 2,6-lutidine and 2,6-di-t-butylpyridine. If there are five sites, calorimetry would group together sites whose enthalpies could differ by 1 or 2 kcal mol^{-1}.

There is speculation in the literature[24,33] that elevated temperatures are needed to access all of the Brönsted sites in HZSM-5. Binding base molecules to Brönsted sites is proposed to block access to other sites. The good agreement between the 0.6 millimoles of sites found in our solution studies at room temperature and the 0.5 milimoles of sites found in the gas phase studies of a similar HZSM-5 sample suggest the base migrates from site to site during the few second time scale of the room temperature, solution calorimetric measurement. After the instantaneous exotherm accompanying base addition, we do not observe the sloping base line that is expected for a reaction proceeding on the time scale of minutes. In NMR studies by these same authors[33] who propose blocked access, it is claimed that site coverages less than one must be used to probe the Brönsted site with acetone to avoid complications[32] by exchange of chemisorbed or physisorbed species and bimolecular reactions.[32] At coverages less than 5 millimoles g^{-1} there is no proof that exchange is not occurring. Chemical shift anisotropies suggest that the exchange reaction could involve segmental motion or that some of the observed anisotropy is due to the small contribution of site 1 to site 2. We conclude, in agreement with other literature reports,[46] that pyridine diffusion through all parts of the structure allows it to interact with all the acid sites relevant to catalysis.

The correlation of enthalpies of adduct formation to spectral changes in donor and acceptor molecules has been established for several solution systems.[34] Studies of spectral shifts in non-coordinating solvents has demonstrated a pronounced effect of the polarity of the medium in many instances.[47] The ^{13}C resonance of acetone, proposed to measure acid site concentration in zeolites, is consistent with 0.5 mmoles g^{-1} of the single

acid sites found for HZSM-5 in gas phase calorimetry studies.[33] Consequently, the reported[33] ^{13}C shift of acetone does not discriminate the differences in the donor-acceptor interaction involving site 1 and site 2. This could result from the sensitivity of the measurement, or rapid exchange of acetone between the two sites or from dominant contributions to the shift by the polarity of the zeolite environment masking the differences in the specific interaction.

The difference in the ^{13}C shift of the α and β carbons of mesityl oxide upon protonation has been used[48] to measure solution acidity. The α proton is influenced slightly by protonation and is used to correct the β-shift for medium effects (i.e., non-specific solvation in solution). In solution, rapid exchange and ion pairing gives rise to concentration dependent shifts which require extrapolation of the shift to infinite dilution. These shifts are expressed as H_o values using a calibration curve of $\Delta\delta°$ vs H_0 values. In solids, the concentration of the strongest site must be large enough to detect. Furthermore, exchange with other strong sites and excess mesityl oxide must be slow on the NMR time scale, in order for the magnitude of this shift difference for site 1 to correlate to ΔH.

Measurement of the temperature programmed desorption of isopropylamine from solid acids has been suggested as a means of measuring the quantity of Brönsted sites on a solid. Weakly bound amine is desorbed by heating at low temperatures. The amount of adsorbate undergoing acid catalyzed decomposition to give alkene and ammonia is reported to provide a measure of the number of strong acid sites. The values reported[33] for HZSM-5 correspond to the sum of n_1 and n_2. If site 2 is a hydrogen bonding site, as cal-ad suggests, it is not expected to cause rearrangement. We propose that the porosity

of the solid keeps the amine bound to site 2 as a reservoir for the acid catalyzed decomposition occurring at site 1. As alkene and ammonia form they are desorbed and replaced on the Brönsted site by amine from site 2. In this manner, the total amount of isopropylamine on site 1 and 2 reacts. Any losely held excess amine is volatilized before degradation temperatures are attained. Providing a reservoir of substrate would be an important advantage of using zeolites in catalysis.

Relationship of Cal-ad and NMR Results

Solid state NMR has been used extensively to probe the reactivity of zeolites and is very important for the characterization of different preparations. ^{1}H, ^{29}Si, and ^{27}Al MAS NMR spectra of our sample of HZSM-5 are given in Figure 2-6. The proton spectrum shown in Figure 2-6 (a) is resolved into three peaks (see Experimental) that are assigned to bridging (AlOH) hydroxyl groups (at 4.0 ppm), hydroxyl groups attached to extra-framework aluminum (at 2.5 ppm) and silanol groups (at 1.7 ppm). These assignments are made on the basis of literature reports.[35] The resolved ^{1}H signal for the bridging (AlOH) at 4 ppm accounts for 27.6% of the total proton spectral area. The resolved silanol peak accounts for 27.3% of the proton spectra giving a bridging framework AlOH to silanol ratio of one. The peak assigned to extra-framework aluminum has a peak area of 37.5% of the signal. A very broad peak results at 6.2 ppm corresponding to 7.6% of the spectral intensity. Framework Al atoms are considered atoms that are tetrahedrally coordinated into the frame structure of the zeolite. Extra-framework Al's are atoms or molecules that are located inside the channels, cages or

voids of the structure. They usually are six-coordinated, but tetra coordination Al can be present at extra-framework locations. As an analogy, extra-framework Al can be considered a guest confined in the cavities of zeolite hosts.

The ^{27}Al MAS NMR spectrum of the HZSM-5 (Figure 2-6 (b)) provides information about framework and non-framework aluminum in the zeolitic structure. Curve resolution shows two lines at 54 and 0 ppm due to four-coordinated framework and six-coordinated extra-framework aluminum, respectively. An additional broad line appears at about 32 ppm which is related to tetrahedral extra-framework Al-OH.[35a,35b] The peak areas indicate 29.1% extra-framework aluminum (lines at 0 and 32 ppm) and 70.9% of framework aluminum (line at 54 ppm). With a bulk Si/Al atomic ratio of 36, the ratio of silicon to framework aluminum atoms is 50.8. An HZSM-5 sample studied by gas solid calorimetry[33d] has 79% framework aluminum in a sample with a bulk Si/Al ratio of 54 and a silicon to framework aluminum ratio of 68.

The number of framework aluminums per unit cell and per gram of solid can be calculated using the unit cell formula for HZSM-5 ($H_nAl_nSi_{96-n}O_{192}$) and the framework Si/Al ratio. For every 50.8 silicon's there is one aluminum giving an empirical formula of $H_{1.9}Al_{1.9}Si_{94.1}O_{192}$ for our sample. In order to compare NMR results with cal-ad results, it would be useful to know the acid site density in mol per gram of HZSM-5 zeolite. Assuming all the framework aluminums lead to acid sites, the site density is obtained by dividing moles of aluminum per unit cell by the M.W. of the unit cell. This leads to 0.32 ± 0.05 millimoles of acid sites per gram. Since the intensity of the

resonance assigned to the AlOH sites in the ^{1}H MAS NMR spectrum is similar to that assigned to the silanol groups there also are 0.32 millimoles of silanols per gram.

None of the strongest sites arise from extra lattice material. γ-alumina is the most acidic form of alumina and its strongest sites are ~ -18 kcal $mole^{-1}$. Thus, non-framework alumina will have little impact on the Cal-ad or catalysis results and at most will block some sites and influence the n-value.

The ^{29}Si MAS NMR spectrum (Fig. 2-6 (c)) shows silicon environments[35] assigned to structurally non-equivalent silicon atoms bonded to other silicons Si(0Al) (i.e., no aluminum attached) at -117.0 ppm and -113.2 ppm. These resonances constitute 14.1% and 71.4% respectively of the total silicon resonance. The Si(1Al) and Si(0Al, 1OH) defect sites have almost identical chemical shifts leading to one resonance whose resolved contribution is 14.1% of the silicon resonance. The Si(1Al) sites are bound to the acidic hydroxyl aluminum centers and are present in a 1:1 ratio to the silanol Si(0Al, 1OH) sites. With 4 silicons bound to each of the 1.9 aluminums in the unit cell, there are 7.6 Si(1Al) and 7.6 Si(0Al, 1OH) per unit cell.

With half the area of the -107.3 ppm resonance or 7.0% of the total silicon resonance due to Si(1Al), the Si/Al framework ratio is given by 100/(0.25 * 7.03) or 56.9 (see Experimental). This result agrees, within experimental error of the resolution, to that obtained from ^{27}Al MAS NMR. The silanol groups correspond to isolated Si-OH functionality with cal-ad enthalpies of binding expected[31] to be < 5 kcal $mole^{-1}$.

The significant aspect of this analysis is that only 19% of the framework AlOH sites lead to the 0.05 millimoles of strong acid sites. The total of the acid sites from cal-

ad ($n_1 + n_2$) equals 0.6 ± 0.2 mmoles per gram which is in reasonable agreement with the 0.3 (± 0.2) millimoles of framework aluminum from NMR. Thus, both sites 1 and 2 for the pyridine reaction arise from bridging Al(OH)Si functionality. Our Si and Al NMR spectra do not distinguish the two types of acid centers arising from framework AlOH groups and unless the very broad proton resonance at 6.2 ppm is due to site 1, proton NMR does not distinguish them. It is significant, that ^{1}H NMR over a range of temperatures probing dipolar coupling to ^{27}Al show two potential Brönsted environments.[49]

Conclusions

The application of the cal-ad method to HZSM-5 extends the enthalpy criterion used to measure solution acidity to zeolites. As in solution, the donor-acceptor component, which is related to bond strength, is best reflected by the enthalpy.[34] The donor-acceptor component is determined and the enthalpy scale from cal-ad provides a temperature independent scale of acidity that establishes HZSM-5 as a strong acid but not a superacid.

Study of the reaction of pyridine with HZSM-5 by cal-ad shows that the 0.6 millimoles of Brönsted sites found with other methods are really 0.0415 millimoles of a strong Brönsted site, $-\Delta H = 42.1 \pm 0.8$ kcal mole^{-1} and 0.53 millimoles of a weaker hydrogen bonding site, $-\Delta H = 8.6 \pm 3.8$ kcal mole^{-1}. For the first time a solid acidity is characterized by K, n and ΔH. This characterization proves that both sites react simultaneously even at lower base concentration. The similarity expected for the K's at

high temperatures accounts for the sites not being distinguished by gas phase calorimetry or temperature programmed desorption measurements.

Cal-ad studies of the reactions with pyridine, 2-6-lutidine and 2,6- di-t-butylpyridine show all of the strong acid sites and most of the weaker sites (-9 kcal mole^{-1}) are located in pockets or corners that exist in the zig-zag, 5.5 Å channel of the zeolite. In addition to surface sites, hydrogen bond sites exist in the straight channels that can be accessed by 2,6-lutidene. Neither the surface sites nor straight channels contain measurable quantity of Brönsted sites.

The cal-ad results reported in this chapter are shown to be consistent with reported experimental observations of zeolite reactivity. Reasons are offered that explain why most of the indirect methods for estimating acidity do not discriminate sites n_1 from n_2 even though enthalpies of binding differ by ~30 kcal mole^{-1}. As a result, an overestimate of the number of strong Brönsted sites in the solid exists in literature reports. The hydrogen bonding sites are suggested to play a role in reactivity by providing a reservoir for reaction at the Brönsted sites.

CHAPTER 3
ACIDITY OF TS-1

Introduction

The success of zeolites in numerous industrial catalytic processes stimulated the search for catalysts containing elements different from Al^{3+} in a silica lattice. These elements could, in principle, impart various catalytic properties to the solid for reactions other than those catalyzed by acids. They may also offer the advantage of atomic dispersion, which is difficult to achieve with traditional preparation methods.[50] The synthesis of TS-1, a titanium derivative of silicalite-1 (MFI structure) with a small fraction of isomorphous framework substitution of Si^{IV} by Ti^{IV} has been reported[51] to form a metallosilicate with no charge on the framework and thus no Brönsted acidity. The structure of TS-1 can be represented as shown in Figure 3-1.

TS-1 has been synthesized by the hydrothermal crystallization of a gel obtained from the reaction of TEOS (tetraethyl orthosilicate) with TEOT (tetraethyl orthotitanate) in the presence of tetrapropylammonium hydroxide (TPA-OH). X-ray powder diffraction indicates that TS-1 possesses the pentasil-type framework similar to that of HZSM-5.[52]

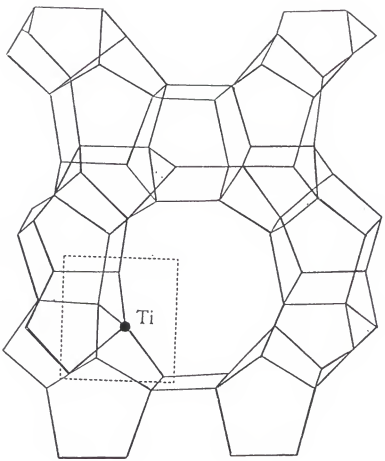

Figure 3-1. Crystalline structure of TS-1.

The isomorphous substitution of Si^{IV} by Ti^{IV} is supported by the gradual increase in unit-cell parameters as the degree of substitution increases.[53] Good agreement between the observed and calculated values of the Si-O (1.61 Å) and Ti-O (1.79 Å) distances support the isomorphous substitution as well. As the amount of substitution increases, a BET surface area increase from 384 m^2/g for silicalite ($Si_{96}O_{192}$) (Si/Ti = ∞) to 485 m^2/g ($Si_{87.67}Ti_{8.33}O_{192}$) (Si/Ti = 10) is reported.[54]

There is a limit to the extent of isomorphous titanium substitution. Attempts to synthesize TS-1 with higher than 3% Ti content result in the formation of TiO_x nanophases. The correlation between Ti content and unit cell volume no longer holds.[55] When extra-framework Ti^{IV} is present, the efficiences of the catalysts in oxidation processes decrease drastically.

The catalytic properties of titanosilicalites are unique. In a variety of liquid-phase oxidation reactions of alcohols, ketones, alkanes, and cyclohexane using H_2O_2 as the oxidant, excellent selectively and only a slight loss of H_2O_2 from decomposition to H_2O and O_2 is observed.[56] Differences in reactivity between small and large alkenes and with H_2O_2 or t-BuOOH as oxidants indicate that the reaction takes place in the channels at titanium sites located in the framework.[55] Silicalite is catalytically inactive,[57] so framework Ti^{IV} is indicated as the catalytic center. Ti^{IV} does not give rise to acidic properties. Higher peroxide efficiencies with catalysts where the TiO_2 phase is absent are attributed[57] to the low activity of Ti^{IV} in the framework positions (tetrahedral coordination) for H_2O_2 decomposition. Shape selectivity, which favors small linear molecules as observed in the low temperature epoxidation of olefins is also observed in

TS-1.[57] Differences between 1-hexene and cyclohexene epoxidations suggest that in many cases the reaction takes place inside the pores, where the majority of the Ti^{IV} is located. However, with larger molecules and at higher temperatures reaction may occur on the Ti^{IV} located on the outer surface of the solid.

The active catalytic centers for oxidation are assigned to isolated Ti^{IV} in an O-Si-O-Si-O silica matrix with no Ti-O-Ti bonds. Two structures have been proposed for isolated Ti^{IV}, the titanyl form I and the tetrahedrally coordinated form II.[58]

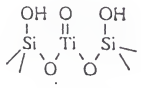

I

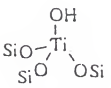

II

The titanyl form I is very unlikely because the typical (>Ti=O) absorption is absent in the UV-VIS spectra of TS-1.[59] Tetrahedral coordination is the more satisfactory possibility. Active centers are not stable entities, on the contrary it is their reactivity that makes TS-1 efficient catalysts. At room temperature, reversible hydrolysis of the Ti-O-Si bond takes place with the formation of Ti-OH and Si-OH groups. With H_2O_2, TiOOH and SiOH form with the former giving rise to the active catalyst center.[59]

An understanding of the reactivity of TS-1 requires an understanding of its hydrophobicity and acidity. Oxidation of 1-hexene and n-octane on TS-1 occurs readily in aqueous or anhydrous solutions of H_2O_2. However, the same reaction with an amorphous, coprecipitated, TiO_2SiO_2 catalyst is inhibited when aqueous H_2O_2 is the

oxidant.[60] TS-1 is reported[61] to be hydrophobic because of selective absorption of organic compounds from water solutions into the zeolite channels. This hydrophobicity is claimed to make TS-1 a highly efficient catalyst for oxidation of organic substrates using aqueous H_2O_2 as the oxidant.[61]

The equilibrium sorption capacity of water is often considered as a measure of the hydrophilic/hydrophobic character of the zeolite. In TS-1 an increase in water sorption capacity with the increased incorporation of the titanium in the silica matrix is observed.[62] Similarly, increases in the sorption capacity of water has been found in a series of ZSM-5 samples with increasing aluminum(III) content.[63] However, when the water sorption capacity of ZSM-5 (Si/Al $\approx$ 40) is compared with that of a titanium silicate (Si/Ti $\approx$ 48), it is found to be considerably larger for ZSM-5($\approx$ 28 molecules/uc) than for TS-1 ($\approx$ 13.52 molecules/uc).[54] The sorption capacity for water in zeolites depends upon the polarity of the Si-O-M linkages formed upon dehydroxylation.[58] The Si-O-Al linkage is more polar than Si-O-Ti and hence the water sorption capacity for ZSM-5 is more than that of TS-1. Although both Si^{IV} and Ti^{IV} are isovalent species, the difference in electronegativity (EN for titanium = 1.32 and for silicon = 1.74) between them imparts polarity to the Si-O-Ti linkage.[58] As titanium replaces Si in the zeolite, the number of Si-O-Ti linkages increases. Therefore, the equilibrium sorption capacity of water with increasing concentration of titanium in the product is a confirmation for the incorporation of titanium species in the silica framework.[57] It is proposed that both the surface silanol (Si-OH) and Si-OH-Ti linkages act predominantly as sorption centers for basic molecules. As discussed earlier, on account of the greater electronegative character of Si^{IV} compared

to Ti^{IV}, Ti-OH groups (or Si-O-Ti linkages) may be more acidic than Si-OH (or Si-O-Si). The number of acidic Ti-OH groups is proportional to the framework titanium. Therefore, as the Si/Ti ratio increases (i.e., Ti decreases), the number of polar Ti-OH (or Si-O-Ti) groups decreases and a decrease in sorption capacity is observed. If only the more polar Ti-OH groups had acted as sorption centers, the sorption capacity of polar probes would have decreased considerably in the case of silicalite. Therefore, surface Si-OH groups must also be acting as sorption centers.

The measurement of acidic properties by the interaction of TS-1 and mixed oxides with NH_3 has been attempted.[64] The results obtained from temperature-programmed desorption (TPD) indicate that NH_3 is more strongly retained by pure TiO_2 than by any of the mixed oxides.[65] It is therefore doubtful that NH_3 absorption can be used to measure acidity in TiO_2-containing materials. This chapter reports measurements of adsorption thermodynamic parameters for TS-1 and determines how these properties influence the unique catalytic reactivity of TS-1.

Experimental

Materials

Sample preparation consisted of drying the solid in flowing O_2 at 400°C for two hours followed by evacuation at 400°C overnight. Elemental analysis performed by the Microanalysis Laboratory at the University of Florida revealed no carbon or nitrogen in the original and calcined samples. Pyridine (Fisher Scientific) was distilled over CaH_2

using a 12 in. Vigreux column and 2,6-lutidine (Aldrich, 97 %) was used as supplied. Hexane (Aldrich, 99%) was distilled over P_2O_5 and stored over 4 Å molecular sieves.

Infrared, Calorimetric and Adsorption Measurements

Calorimetric, infrared, and adsorption studies were performed on a commercial sample of TS-1 containing 1% titanium by weight. The description of these measurements as well as cal ad analysis was described in Chapter 2.

Results and Discussion

Sample Characterization

The synthesis of TS-1 is difficult to control leading to variation in reactivity and selectivity for different samples.[57] Accordingly, effort was expended to characterize the sample used in this work. The infrared spectrum of our commercial TS-1 sample contains a broad adsorption band at 3400 cm^{-1} due to water and broad silanol bands at 3680 cm^{-1}, Figure 3-2. After drying for 24 hours at 400 °C under vacuum, a sharp band remains at 3694 cm^{-1}. A band at the same frequency is present in HZSM-5 and is assigned to isolated polar silanol groups.[66] When this sample is titrated with pyridine, the band at 3694 cm^{-1} disappears and two bands appear in the pyridine region (1800 - 1450 cm^{-1}) that have been assigned to hydrogen bond sites (pyridine adducts at 1600 and 1573 cm^{-1}) as shown in Figure 3-3. Peaks characteristic of pyridinium ions were not observed indicating the absence of Brönsted acid sites in the TS-1 samples.

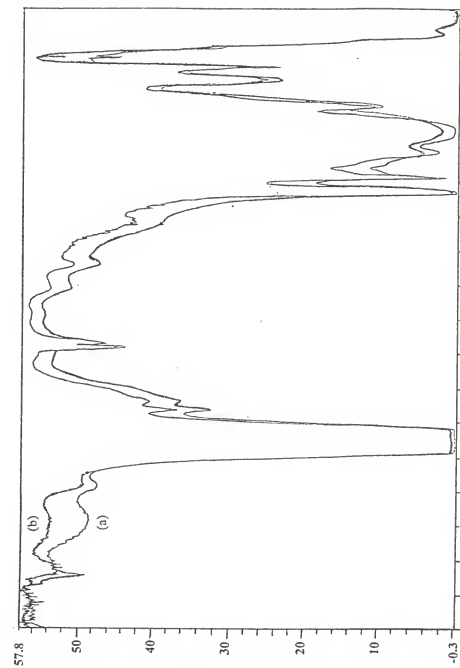

Figure 3-2. FTIR Spectra in Nujol Mulls of TS-1 (a) as Received and (b) After Drying at 400 °C in Vacuum.

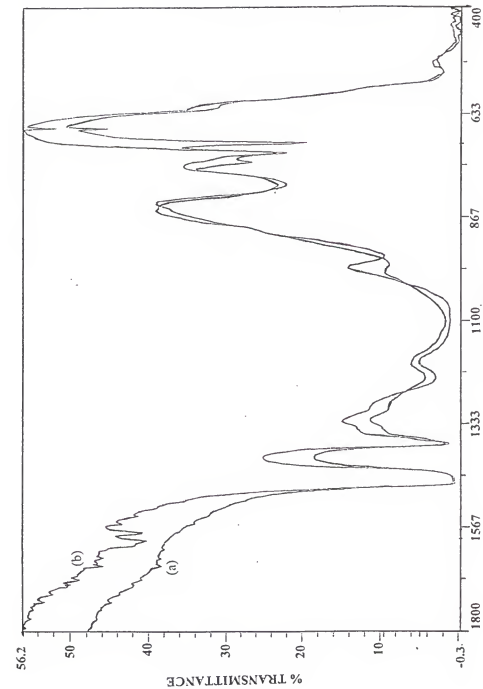

Figure 3-3. FTIR Spectra in Nujol Mulls of TS-1 (a) Dried and (b) After Calorimetric Titration with Pyridine.

Titanium silicates exhibit an IR band at 960 cm^{-1}, characteristic of the stretching mode of a [SiO_4] unit bonded to a Ti^{IV} ion or a titanyl group (>Ti = O), (as(O_3Si-O-Ti)) suggesting the presence of tetrahedral titanium in the zeolite framework. This band is not observed in the IR spectra of HZSM-5 (Figure 3-4). Upon hydrogen bonding to pyridine, a shift of this Si-O-Ti stretching vibration to higher energy occurs. In addition, a band at ~1100 cm^{-1} is assigned as asymmetric Si-O-Si network vibration with the corresponding symmetric vibration at around 800 cm^{-1}.

Cal-ad Results

A cal-ad analysis of a commercial sample of TS-1 containing 1% titanium by weight was carried out. Pyridine and 2,6-lutidine were selected as donors in order to avoid the amphoteric interaction encountered when protonic donors (e.g. NH_3) are studied.

The pyridine and 2,6-lutidine adsorption isotherms for TS-1 are shown in Figure 3-5 and 3-6 where the millimoles of base adsorbed by one gram of the solid slurried in 100 ml of hexane are plotted vs the equilibrium amount of base in solution. Figures 3-5 and 3-6 also give the results for the calorimetric titration by plotting the sum of heat evolved h' versus moles of base added to one gram of TS-1 slurried in 100 ml of hexane.

Figure 3-7 is a plot of the average enthalpies of reactions for pyridine and 2,6-lutidine with TS-1. The average enthalpies are calculated using a limited reagent assumption by dividing h' by the moles of base added. Therefore these results are averages of the sites that react with each incremental addition of base.

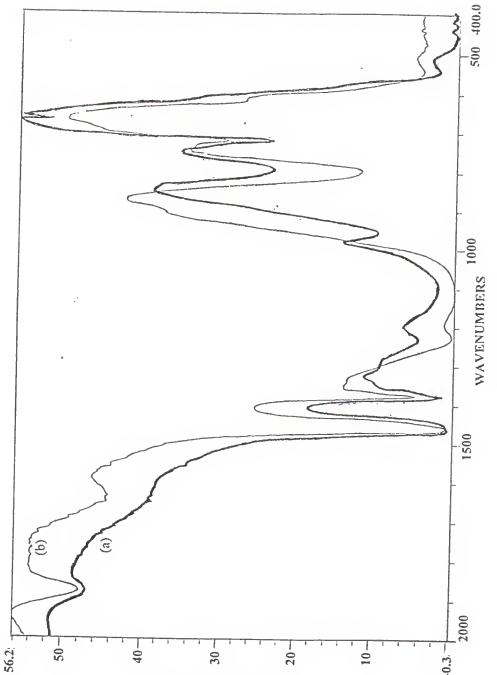

Figure 3-4. FTIR Spectra in Nujol Mulls of (a) TS-1 and (b) HZSM-5 Dried.

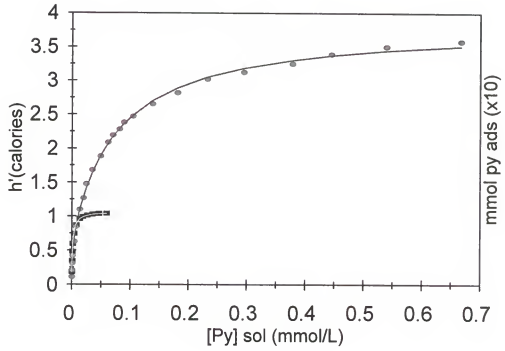

Figure 3-5. Adsorption isotherm and heat of adsorption versus concentration of pyridine in solution: (■) calorimetric points, (●) adsorption data points, and (—) solid line: calculated using values from Table 3-1.

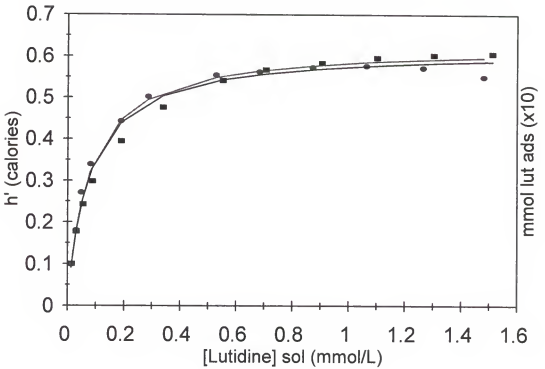

Figure 3-6. Adsorption isotherm and heat of adsorption versus concentration of 2,6-lutidine in solution: (■) calorimetric points, (●) adsorption data points, and (—) solid line: calculated using values from Table 3-1.

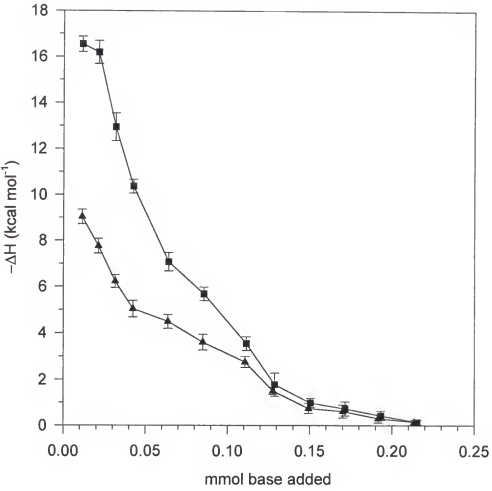

Figure 3-7. Average enthalpies of reactions versus mmol of base added.
■ pyridine, ▲ 2,6-lutidine

The results of the cal-ad analysis of TS-1 are given in Table 3-1. In Figure 3-8, the dots indicate the experimental h' values as the sum of heat evolved for incremental additions of pyridine to one gram of TS-1 in hexane.

Table 3-1. Thermodynamic parameters obtained in hexane solvent for reactions of TS-1 (1% Ti) with pyridine and 2,6-lutidine.

	Pyridine	Lutidine
n_1 (mmol/g)	0.070 ± 0.005	0.063 ± 0.004
K_1 (M^{-1})	$6.7x10^5 \pm 2.2x10^4$	$1.3x10^4 \pm 3.7x10^2$
$-\Delta H_1$ (kcal/mole)	15.1 ± 0.4	9.8 ± 0.5
$-\Delta G_1$ (kcal/mole)	7.95 ± 0.1	5.61 ± 0.1
ΔS_1 (cal/deg.mole)	-24 ± 1.3	-14 ± 1.7
n_2 (mmol/g)	0.31 ± 24	
K_2 (M^{-1})	$1.3x10^4 \pm 1.1x10^5$	
$-\Delta H_2$ (kcal/mole)	0.02 ± 2.4	
$-\Delta G_2$ (kcal/mole)	5.60 ± 5.0	
ΔS_2 (cal/deg.mole)	19 ± 18.6	

The solid line illustrates the data fit from the cal-ad K's, n's and ΔH's. The fit of the adsorption isotherm is given by the solid line in Figure 3-5. Using the data in Table 3-1, the experimental curve can be separeted into the two contributions from site 1 and 2. The contribution of site 1 is predominant, where the dashed line is superimposed on the experimental curve. The second site does not contribute to all measured h' values as can be seen from the line parallel to zero axis in Figure 3-8.

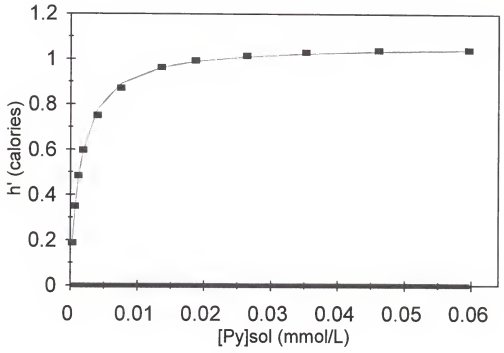

Figure 3-8. Sum of heat evolved versus concentration of pyridine in solution for two acid sites: (■) calorimetric data points, (--) dashed line(under solid line): site 1 and bold line: site 2. Solid line: calculated using values from Table 3-1.

Comparison of the enthalpy of interaction of pyridine for the first site of TS-1 with the enthalpy of reaction of pyridine with HZSM-5[66] (-42 kcal $mole^{-1}$) shows that TS-1 does not have the very strong acid sites of HZSM-5 but is about as acidic as conditioned silica gel[31] (-12 kcal $mole^{-1}$). Thus TS-1, like silica gel, has only silanol hydrogen bonding sites. The n-values from cal-ad are particularly informative. Considering 1% titanium by weight, the sample has 0.23 millimoles of Ti per gram and an empirical formula $Ti_{0.01}Si_{95.99}O_{192}$. The n_1 value of 0.07 millimoles g^{-1} of hydrogen bonding sites in TS-1 is much less than the amount of titanium and the 0.6 millimoles of acid sites (above 10 kcal $mole^{-1}$) in HZSM-5. A comparison of the pyridine cal-ad n_1 for TS-1 (0.07 mmol) and silica gel evacuated at 200°C (n_1 = 1.12 mmol) shows that silica gel also has a larger number of hydrogen bonding sites than TS-1.

The pyridine second site values for TS-1 are attributed to physisorption and the parameters are not well defined. Pyridine is competing with solvent for non-specific adsorption. At the highest concentration employed to measure the adsorption isotherm, only 0.4 millimoles of pyridine are added and this amount is insufficient to define the process parameters in the data analysis.

The titration of TS-1 with 2,6-lutidine gave a similar number of acid sites as pyridine (n = 0.06 millimoles/g). This indicates that vacant metal centered Lewis sites do not exist. The lower enthalpy for 2,6-lutidine compared to pyridine suggests that some of the stronger hydrogen bonding sites in the distribution are not accessed by 2,6-lutidine or ion-pairing is less energetic.

Comparison of the n_1 value for pyridine with that for process 1 for gas adsorption of dimetyl ether on TS-1[67] (0.15 ± 0.04 millimoles g^{-1}) confirms the assignment of this process to hydrogen bonding. Thus the cal-ad results indicate that the absence of acid sites in TS-1 leads to less capacity for water adsorption for TS-1 than HZSM-5 or silica and causes TS-1 to be less hydrophillic.

Conclusions

Liquid phase measurements have been used to probe the cause of the unique catalytic reactivity of TS-1.

The cal-ad method, using combined calorimetric and liquid adsorption studies, has determined that for the donor-acceptor interaction between the acidic sites of TS-1 and pyridine, only 0.07 millimoles per gram of a hydrogen bonding sites ($-\Delta H_1 = 15.1$ kcal mol^{-1}) exist on TS-1 compared to 0.6 mmol g^{-1} for HZSM-5. A second site (0.3 millimoles) is assigned to a physisorption process ($-\Delta H_1 = 0.02$ kcal mol^{-1}).

Comparison of cal-ad studies of the reaction of TS-1 with pyridine to HZSM-5 and silica gel show that TS-1 and silica gel do not present very strong acid sites. The results also indicate a reduced amount of hydrogen bonding functionality on the interior and exterior surface of TS-1 compared to HZSM-5 or silica gel. Thus, the absence of surface acidity (strong acid and hydrogen bonding), instead of an increased dispersion interaction is the cause of the hydrophobic properties of TS-1 compared to HZSM-5.

CHAPTER 4
MEASUREMENTS OF ACIDITY OF Y ZEOLITES

Introduction

Synthetic faujasites (zeolites X and Y) have been studied extensively because of their catalytic applications in hydrocarbon cracking.[68] The use of Y zeolite based catalysts is predominantly in Fluidized Catalytic Cracking (FCC).[69] In 1959 Union Carbide commercialized Y zeolite for the isomerization of pentane and hexane.[6,70]

The use of synthetic faujasites as cracking catalysts was hindered by their poor steam stability. Hydrothermally stabilized Y zeolite and rare-earth-exchanged zeolites were first synthesized in the early 1960's.[7] The discovery of dealuminated Y zeolite (LZ-210) contributed greatly to both the thermal stability and increased selectivity of the zeolite with respect to high-octane gasoline.[70] The dealuminated Y zeolite LZ-210 has a low sodium and aluminum content, and variable SiO_2:Al_2O_3 ratio. Under steaming less debris is formed in the pores leading to a significant enhancement in the selectivity to primary products and to gasoline.

There are two procedures for dealumination of zeolites: chemical and hydrothermal. The chemical dealumination occurs by using a suitable reagent in solution (acids, salts, chelanting agents) or in the vapor phase ($SiCl_4$).[71] Hydrochloric acid, chromium chloride, ammonium fluorosilicate have been employed in solution. The

aluminum is extracted from the lattice, leaving a nest of hydroxyl groups. Further calcination at temperatures as high as 500 or 600°C eliminates these hydroxyl groups and presumably leads to silicon transport to fill the vacancies formed, Si atoms replacing the missing Al atoms, or to reconstruct the lattice. Another dealumination process is hydrothermal treatment. The samples are heated at 600-700°C under N_2 flow saturated with water vapor. Al atoms are extracted from the framework and an Al-O compound is deposited in the cavities or channels.[72] The structure of this Al-O compound is unknown.

Very high extents of dealumination can be obtained by carrying out successive hydrothermal and chemical treatments. The chemical reagent is often hydrochloric acid which dissolves the Al-O compound formed by hydrothermal treatment.[73] Cycling these procedures several times allows one to obtain highly dealuminated zeolites.

The structure of Y zeolites consists of a negatively charged, three-dimensional framework of SiO_4 and AlO_4 tetrahedra, joined to form an array of octahedra.[74] Figure 4-1 shows an example of condensation of the AlO_2^- and SiO_2 units into a 60-atom (silicon, aluminum, and oxygen atoms) sodalite cage, which geometrically is a truncated octahedron. The upper-right-hand portion of Fig. 4-1 shows only the 24 metal atoms that make up the sodalite cage. The 36 oxygen atoms connecting these metal atoms (middle, *top* of Fig. 4-1) make up the remainder of the 60 atoms in the polyhedron.[75] These truncated octahedra (β-cages or sodalite cages) are joined at the octahedral faces by hexagonal prisms resulting in tetrahedral stacking. This type of stacking creates large cavities (α-cages or supercages) with a diameter of ~13 Å. The supercages can be entered through any of four tetrahedrally distributed openings (12-membered rings), each having

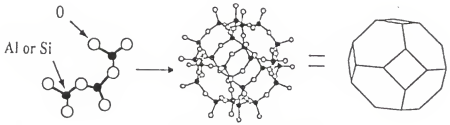

60 atom sodalite cage

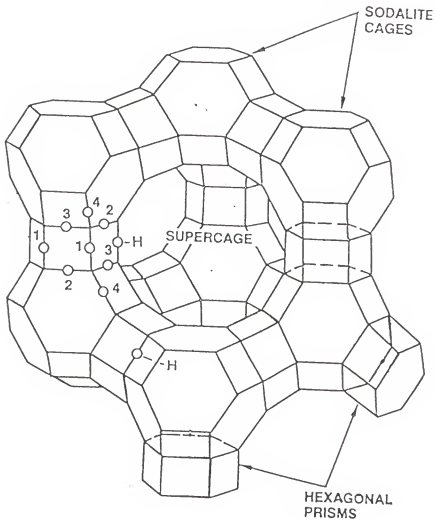

Figure 4-1. Faujasite framework showing oxygen type (O).

a diameter of 7.4 Å. The supercages, connected through 12-membered rings, form the large-pore system of the zeolite (Figure 4-1). The structure also comprises a small-pore system, made up of sodalite cages and the connecting hexagonal prisms. The six-membered rings of the sodalite cages have a diameter of ~2.4 Å. A typical unit cell content of HY zeolite[76] is $H_{56}[(AlO_2)_{56}(SiO_2)_{136}].250H_2O$.

Each tetrahedrally coordinated aluminum atom in the framework carries a negative charge. These negative charges in the framework are compensated by cations located in specific non-framework positions.[77] In the dehydrated form, charge-balancing protons occupy preferred positions in the zeolite and form two types of acidic hydroxyl groups: α-cage hydroxyls (supercage), which are very acidic and are direct accessible to adsorbates; and β-cage hydroxyls (sodalite cage), which are less acidic but sufficiently mobile to interact with α-cage restricted adsorbates. In the hydrated form, the ions and the water molecules in the supercages have considerable freedom of movement, which permits ion exchange, as well as reversible dehydration and sorption.

It is important to note that the ion exchange process can yield very different locations of cations depending on temperature, pH, other extra-framework ions, calcination, loading levels and use of solvent for exchange.

The intracrystalline channel cavity-pore-cage system in zeolites is surrounded by the lattice and therefore is submitted to the zeolite crystal field. This results in solvent-like and even electrolyte-type properties.[78] Cations are easily exchangeable and an interaction may exist between an occluded ionic compound and the zeolitic framework. Salts, especially salts of univalent anions, have been shown to penetrate the zeolite

structure and fill the available space even if the openings of the cavities (as the O_6-ring of 0.24 nm in size in sodalite cage of Y zeolite) is smaller than the size of the anion (ClO^-_3, NO^-_3 for instance).[11] This leads to enhanced thermal stability of the occluded salt.

The correlation of reactivity to acidity is desirable since it is known that different strength acid sites are needed for different acid catalyzed reactions. Various methods have been reported to measure the acidity of solids. The most conventional procedures for study of the acidity of zeolites involve thermal gravimetric (TGA), differential scanning calorimetry (DSC), and temperature-programmed desorption (TPD).[79,80] These techniques measure the interaction of gaseous molecules with a solid surface. The equilibrium data include contributions from donor-acceptor, dispersion and non specific polar interactions of the adsorbate with the surface of the solid. The first limitation of these techniques is the inability to discriminate the type of interaction. Another shortcoming of TGA, DSC, and TPD is the inability of these methods to resolve sites of different acidities. Instead, a weighted average value of K and ΔH results, and several sites are counted as one. The cal-ad method has been shown to discriminate between different acceptor sites that are usually averaged into one site by TGA and DSC.[25]

This chapter will present the results from cal-ad studies for Y zeolite. Reactions with different bases have been investigated to determine the influence of the base on the coordination towards the zeolite. The enthalpies of donor-acceptor interactions and E_B and C_B values for the donors were substituted into the ECW equation[34] to produce a series of equations that was solved for E_A and C_A. By studying the acidity of the solid

towards pyridine, 2,6-lutidine, and 2,6-di-tert-butylpyridine, proton sites can be distinguished from metal centered sites.

Experimental

Materials

Characterization of four Y zeolites with different Si/Al ratios was carried out. Three samples were obtained from PQ corporation and one from Aldrich. Table 4-1 lists reported properties of the samples. Infrared, calorimetric and adsorption studies were carried out on samples that were dried under flowing oxygen for two hours at 450 °C, and then evacuated at 450 °C overnight. The oxygen flow was used to assure that no organic material was present in the samples. During the evacuation period, argon was flushed for 30 minutes and then the system was evacuated again. The drying apparatus used for calcination is shown in Figure 4-2. Finally, the drying apparatus was cooled, filled with argon and transferred to a dry box to load the calorimetric cell. Elemental analyses, performed by the Microanalysis Laboratory at the University of Florida, showed the absence of carbon and nitrogen in the original and calcined samples

Pyridine (Fisher) was distilled over CaH_2 using a 12 in. Vigreux column. 2,6-lutidine (Aldrich, 97 %), 2,6-di-tert-butylpyridine (Aldrich, 97 %), benzonitrile (Aldrich, 99 %), quinoline (Aldrich, 98 %), and tetrahydrothiophene (Aldrich, 99 %), were used as supplied. Hexane (Aldrich, 99%) was distilled over P_2O_5 and stored over 4 Å molecular sieves.

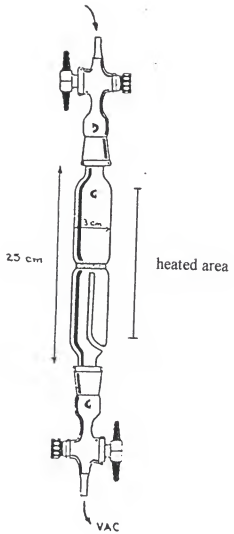

Figure 4-2. Drying Aparattus Used for Calcination of Samples.

Table 4-1. Reported properties of Y zeolites.

Source	SiO_2/Al_2O_3 molar ratio	Na_2O wt%	surface area m^2/g
VALFOR CP300-26	60	0.03	750
(Lot # 9107786K)			
VALFOR CBV 500	5.4	0.2	750
(Lot # 9106694K)			
VALFOR CBV 712	12	0.05	730
(Lot # 9106695K)			
Aldrich LZ-Y62	2.9	2.5	
(Lot # 00220BZ)			

Infrared, Calorimetric and Adsorption Measurements

The description of these measurement techniques used for the experiments have been described in Chapter 2.

Thermogravimetric Analysis

TG studies were performed with the aid of Dr. K. Williams on a Dupont 2000 instrument (module 2950) with Ar as the carrier gas. Samples were ramped from room temperature to 800 °C at 10 °C per minute. The samples were taken directly from the bottle.

Neutron Activation Analysis

NAA studies were performed with the aid of Dr. K. Williams. Samples and standards were sealed in polyethylene vials for use in the rabbit system.[81] The aluminum standard was reagent-grade $Al(NO_3)_3.9H_2O$ (Mallinckrodt), and the silicon standard was pure silicon solid powder (Johnson Matthey, 99.99%, 325 mesh). Samples and standards were activated for 45 sec. in the University of Florida Training Reactor at the maximum power of 100 kW. For the irradiations, a pneumatic rabbit system was used to transport the vials to and from the reactor core. The samples were inserted via the reactor's center vertical port, prior to raising the power. The fluxes in this region of the reactor are about 1.3×10^{12} and 1.0×10^{11} cm^2s^{-1} for thermal and higher energy neutrons, respectively.

After removal from the reactor and cooling as needed, the samples and standards were counted using an EG&G ORTEC germanium detection system. Both n-type (23%) and p-type (23%) crystals were utilized. All counting data were corrected for decay during cooling and during the counting period, as well as for the dead time of the detector.

Inductive Coupled Plasma Analysis

ICP studies were performed with the aid of Dr. Geraldo Boaventura (Universidade de Brasilia, Brazil) on a Spectroflame FVM3-90/2217 with argon as the carrier gas, focal distance of 75 cm, Paschen-Runge setting, monocromator in air for the range 210 nm to 480 mm and a Meinhard nebulizator. Fusion with $LiBO_2$ (lithium metaborate) in platinum crucible was used to determine Si and Al, following the procedure of

Ingamells[82]. After preparation of samples, measurements of emission intensities were done on the instrument using calibration curves with one blank and 5 (five) standard solutions for each element. The wavelength and detection limits obtained were

	λ (nm)	limit of detection (mg/l)
Si	251.61	0.111
Al	308.21	0.037

Atomic Absorption Spectroscopy Analysis

AAS studies were performed with the aid of Dr. Geraldo Boaventura on a Perkin Elmer 3100 using the same solutions as in the ICP analyses.

X-Ray Diffraction analysis

XDR studies were performed by Major Analytical Instrumentation Center of the University of Florida using a 40 kV, 40 mA. Scanned at steps of 0.050 with count time of 0.5 seconds per step.

Results and Discussion

ICP, NAA, and Elemental Analysis

Y zeolites obtained from PQ Corporation were synthesized at low Si/Al ratios (approximately 2) and then dealuminated by acid treatment. The results from

measurements of the Si and Al percentages by ICP and NAA for Y zeolites as received are shown on Table 4-2. Good agreement is obtained between the techniques.

Table 4-2. ICP and NAA analysis for Y zeolites.

	% Si		% Al		Si / Al	
Source (Si/Al)	ICP	NAA	ICP	NAA	ICP	NAA
Aldrich (2.5)	25.25	23.74	9.36	11.24	2.69	2.11
PQ (5)	29.92	35.47	10.11	11.86	2.97	2.99
PQ (10)	37.56	39.88	5.56	4.97	6.76	8.02
PQ (89)	40.39	42.36	0.81	0.96	49.86	44.1

Using the same solutions from ICP analysis the Na content was determined by atomic absorption for Y zeolites. The results are shown in Table 4-3.

Table 4-3. AAS analysis for Y zeolites.

Si/Al	% Na
2.7	1.93
3.0	0.50
6.8	0.29
50	0.08

The lower % Na for higher Si/Al ratio is explained by the need for less charge compensation when aluminum is removed from the structure.

Elemental analyses of the Y zeolite samples as received (from bottle) and after calcination are presented in Table 4-4.

Table 4-4. Elemental Analysis of Y zeolites.

	Si / Al = 2.7		Si / Al = 3.0		Si / Al = 6.8		Si / Al = 50	
	bottle	450^0C	bottle	450^0C	bottle	450^0C	bottle	450^0C
% C	—	—	—	—	—	—	—	—
% N	4.84	—	1.46	—	0.46	0.02	—	—
% H	2.82	0.52	2.21	1.91	1.16	0.77	0.30	0.34

The Y zeolite (Si/Al = 2.7 from Aldrich) has a large amount of nitrogen that is removed by the calcination procedure.

TGA and XRD Studies

In order to study the loss of water by the four samples, thermogravimetric analysis were carried out. All thermograms (Figures 4-3 through 4-6) exhibited a mass loss attributed to occluded water between room temperature and ca. 200°C.

The X-ray diffraction analysis for Y zeolites samples are presented on Figures 4-7 through 4-10. The plots show that all the samples have a high degree of cristallinity. XRD on the sample with a Si/Al ratio of 6.8 as received and after calcination (Figures 4-9 and 4-10) is essentially unchanged.

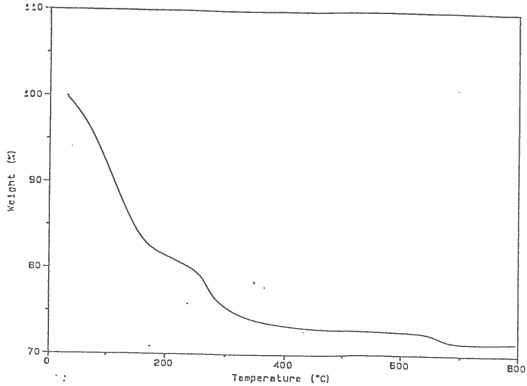

Figure 4-3. TGA Plot of Y Zeolite (Si/Al = 2.7) from bottle.

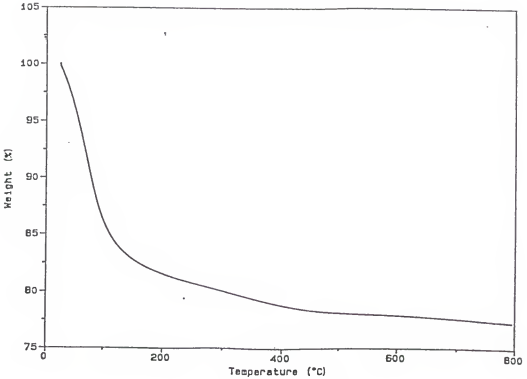

Figure 4-4. TGA Plot of Y Zeolite (Si/Al = 3.0) from bottle.

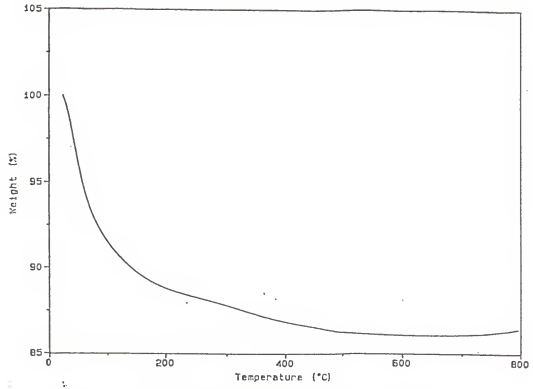

Figure 4-5. TGA Plot of Y Zeolite (Si/Al = 6.8) from bottle.

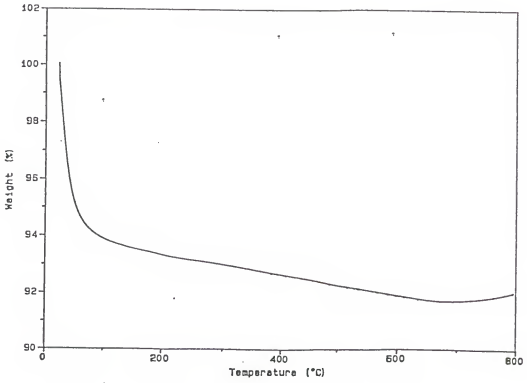

Figure 4-6. TGA Plot of Y Zeolite (Si/Al = 50) from bottle.

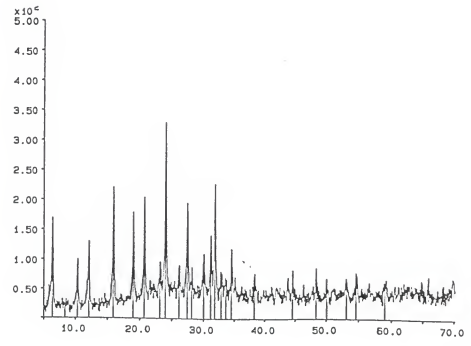

Figure 4-7. XRD Plot of Y Zeolite (Si/Al = 3.0) Dried at 450 °C.

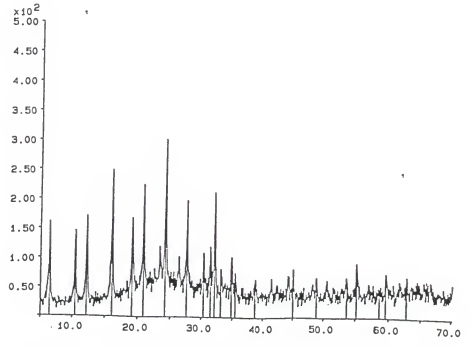

Figure 4-8. XRD Plot of Y Zeolite (Si/Al = 50) Dried at 450 °C.

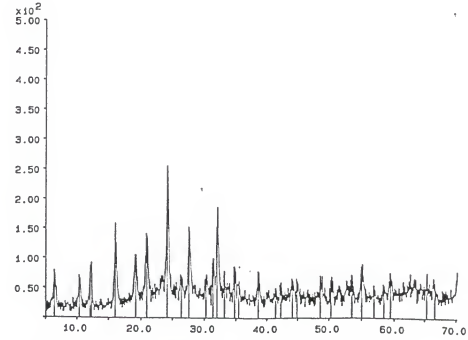

Figure 4-9. XRD Plot of Y Zeolite (Si/Al = 6.8) from Bottle.

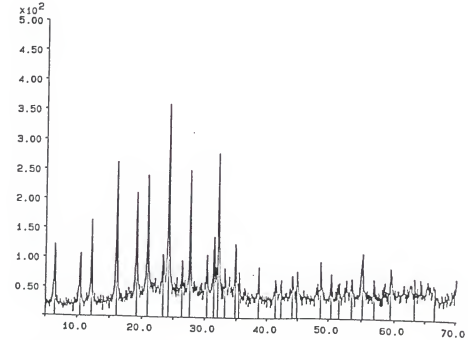

Figure 4-10. XRD Plot of Y Zeolite (Si/Al = 6.8) Dried at 450 °C.

Infrared Studies

Zeolites have high affinity for water and precautions must be taken to dry the samples and to exclude water during the measurements. Figures 4-11 through 4-14 show the infrared spectra of the samples received and those after drying for 24 hours at 450°C under vacuum with periodic flushing of the apparatus with argon. After drying, the Y zeolite (Si/Al = 2.7 - Figure 4-11) shows a sharp band at 3540 cm^{-1} which is attributed to the bridging Al-(OH)-Si acid sites. Figure 4-12 (Y, Si/Al = 3.0) is a less concentrated mull that also shows the broad band at 3528 cm^{-1} attributed to the Al-(OH)-Si sites. Figure 4-13 (Y, Si/Al = 6.8) shows two bands after drying: a sharp one at 3694 cm^{-1} and a broad band at 3524 cm^{-1}. The former is attributed to nested silanols formed as consequence of dealumination process. The band at 3524 cm^{-1} is attributed to the Bronsted bridging Al-(OH)-Si sites. Figure 4-14 (Y, Si/Al = 50) show one sharp band at 3690 cm^{-1}, attributed to the nested silanols. The band for Al-(OH)-Si sites is not detected by IR because of the low concentration of these sites on this highly dealuminated sample. A comparison of Figures 4-11 through 4-14 show that as the dealumination ratio (higher Si/Al ratio) increases the Al-(OH)-Si band decreases while the nested silanol band increases.

When a samples of Y with a Si/Al ratio of 3.0 was deuterated and dried, the broad band at 3528 cm^{-1} shifts to 2647 cm^{-1}(Figure 4-15).

When all these samples are titrated with pyridine in a calorimetric run, the spectrum of the resulting solid shows no adsorption in the OH region but has bands in the pyridine region (1700-1300 cm^{-1}). Figure 4-16 shows the IR spectra from Y zeolites (Si/Al = 2.7, 3.0 and 6.8). The bands at 1545 and 1489 cm^{-1} have been assigned to the

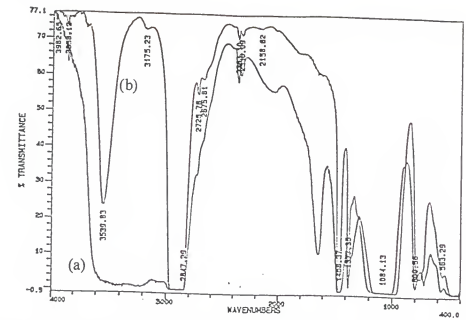

Figure 4-11. FTIR Spectra of Y Zeolite (Si/Al = 2.7) from (a) bottle and (b) Dried at 450 °C.

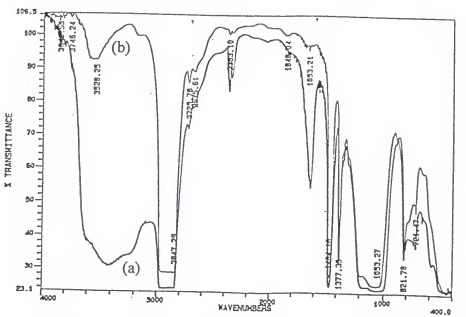

Figure 4-12. FTIR Spectra of Y Zeolite (Si/Al = 3.0) from (a) bottle and (b) Dried at 450 °C.

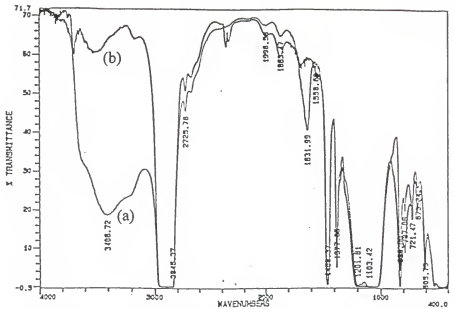

Figure 4-13. FTIR Spectra of Y Zeolite (Si/Al = 6.8) from (a) bottle and (b) Dried at 450 °C.

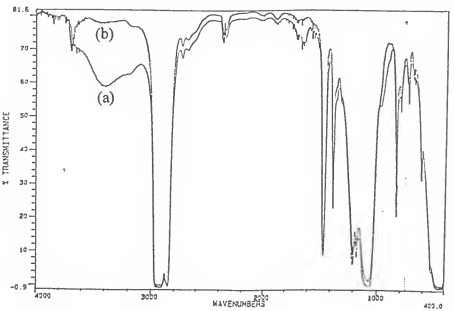

Figure 4-14. FTIR Spectra of Y Zeolite (Si/Al = 50) from (a) bottle and (b) Dried at 450 °C.

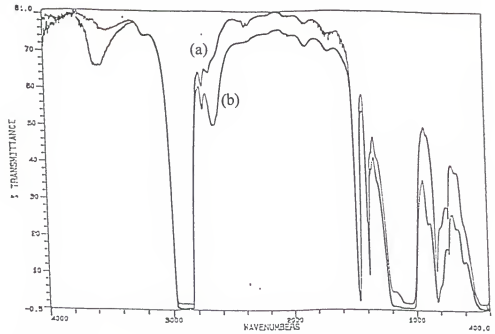

Figure 4-15. FTIR Spectra of Y Zeolite (Si/Al = 3.0) (a) Dried at 450 °C and (b) after Deuteration.

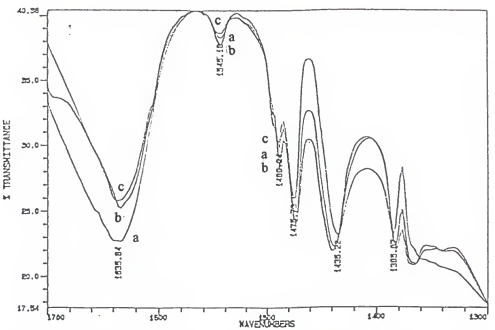

Figure 4-16. FTIR Spectra of Y Zeolites After Calorimetric Experiment (a). Si/Al = 2.7; (b). Si/Al = 6.8; (c). Si/Al = 3.0.

pyridinium ion and the band at 1636 cm^{-1} is attributed to pyridine hydrogen bond adduct. Both interactions are observed in all samples.

Cal-ad Results

The calorimetric titration of three samples of Y zeolite (Si/Al = 3.0, 6.8 and 50) with pyridine are shown in Figure 4-17 where the heat evolved is plotted vs. the amount of pyridine added to one gram of zeolite slurried in 100 ml of hexane. The adsorption measurements of pyridine by Y zeolites (Si/Al = 3.0, 6.8 and 50) are shown in Figure 4-18 where the millimoles of pyridine adsorbed by one gram of the solid slurried in 100 ml of hexane is plotted vs. the amount of pyridine added. The concentration of the pyridine reactant solution is 0.1 M. The higher the Si/Al ratio, the lower the millimoles of pyridine adsorbed. This is expected because Al is responsible for the acid sites and dealumination reduces the number of acid sites.

Y zeolite (Si/Al =6.8) was chosen for characterization with the cal-ad analysis because this sample gave the highest heat evolution in the reaction with pyridine. The resulting thermodynamic values for the reactions of Y zeolite (Si/Al = 6.8) with pyridine, 2,6-lutidine, 2,6 di-t-butylpyridine, quinoline, tetrahydrothiophene and benzonitrile are given in Table 4-5.

The main conclusions are obtained from number of sites and enthalpies. Titrations of Y zeolite (Si/Al = 6.8) with pyridine and 2,6-lutidine gave similar number of acid sites (n_1 = 0.1 mmol) and enthalpies of 34.1 and 30.8 kcal mol^{-1}, respectively. This suggests that both probes are titrating sites inside the large cages. The second sites for

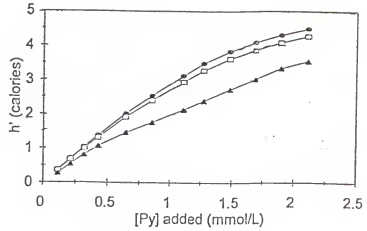

Figure 4-17. Heats of Adsorption of Pyridine for Y Zeolites (□ Si/Al = 3.0), (● Si/Al = 6.8) and (▲ Si/Al = 50).

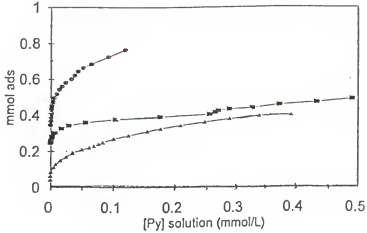

Figure 4-18. Isotherms of Adsorption of Pyridine for Y Zeolites (● Si/Al = 3.0), (■Si/Al = 6.8) and (▲ Si/Al =50).

Table 4-5. Thermodynamic Parameters Obtained in Hexane Solvent for Reactions of Y (Si/Al = 6.8) with Pyridine, 2,6-Lutidine, 2,6-di-t-butylpyridine, Quinoline, Tetrahydrothiophene and Benzonitrile.

	Pyridine	2,6-Lutidine	2,6-di-t-butylpyridine
n_1 (mmol/g)	0.108 ± 0.0023	0.106 ± 0.0024	0.205 ± 0.0023
K_1^{298} (M^{-1})	$2.1x10^8 \pm 2.1x10^6$	$1.9x10^7 \pm 1.2x10^5$	$2.0x10^6 \pm 1.3x10^5$
$-\Delta H_1$ (kcal/mol)	34.08 ± 0.20	30.85 ± 0.17	18.8 ± 2.20
$-\Delta G_1^{298}$ (kcal/mol)	11.35 ± 0.1	9.93 ± 0.1	8.60 ± 0.1
ΔS_1 (cal/deg.mol)	-76 ± 0.7	-70 ± 0.6	-34 ± 7.4
n_2 (mmol/g)	0.22 ± 0.17	0.20 ± 0.04	
K_2^{298} (M^{-1})	$1.4x10^6 \pm 1.1x10^6$	$3.4x10^5 \pm 6.9x10^4$	
$-\Delta H_2$ (kcal/mol)	17.7 ± 7.6	13.1 ± 1.7	
$-\Delta G_2^{298}$ (kcal/mol)	8.38 ± 0.5	7.55 ± 0.1	
ΔS_2 (cal/deg.mol)	-31 ± 25.5	-19 ± 5.7	
	Quinoline	Tetrahydrothiophene	Benzonitrile
n_1 (mmol/g)	0.050 ± 0.012	0.052 ± 0.0019	0.096 ± 0.0023
K_1^{298} (M^{-1})	$6.3x10^6 \pm 3.5x10^5$	$6.6x10^7 \pm 1.0x10^6$	$1.6x10^7 \pm 7.6x10^5$
$-\Delta H_1$ (kcal/mol)	32.13 ± 1.4	29.05 ± 0.46	13.16 ± 0.59
$-\Delta G_1^{298}$ (kcal/mol)	9.28 ± 0.1	10.67 ± 0.1	9.83 ± 0.1
ΔS_1 (cal/deg.mol)	-77 ± 4.7	-62 ± 1.5	-11 ± 2.0
n_2 (mmol/g)	0.75 ± 0.32	0.23 ± 0.09	0.38 ± 0.20
K_2^{298} (M^{-1})	$6.8x10^4 \pm 2.9x10^4$	$7.9x10^5 \pm 3.4x10^5$	$5.4x10^5 \pm 2.8x10^5$
$-\Delta H_2$ (kcal/mol)	9.2 ± 5.2	7.2 ± 3.7	4.3 ± 3.3
$-\Delta G_2^{298}$ (kcal/mol)	6.59 ± 0.3	8.05 ± 0.3	7.82 ± 0.3
ΔS_2 (cal/deg.mol)	-9 ± 17.5	3 ± 12.4	12 ± 11.1

pyridine and 2,6-lutidine along with the first site for 2,6 di-t-butylpyridine present similar n's (0.22, 0.20 and 0.21 mmol, respectively) and ΔH's (17.7, 13.1 and 18.8 kcal mol^{-1}, respectively). This suggests that the second sites for pyridine and 2,6-lutidine along with the first site for 2,6 di-t-butylpyridine are located near to the surface of the solid.

The cal-ad results for quinoline show comparable enthalpies (ΔH_1 = 32.1 kcal mol^{-1}) to the first site of pyridine (ΔH_1 = 34.1 kcal mol^{-1}) but the number of quinoline sites is half that for pyridine. This is explained by the larger size of quinoline than pyridine. Coordinated quinoline molecules block access of other quinoline molecules to adjacent acid sites. Tetrahydrothiophene shows similar results to quinoline, indicating that the same acid sites are inaccessible. Finally, benzonitrile presents a n_1 comparable to pyridine (0.1 mmol) but the enthalpy is much lower (ΔH_1 = 13.1 kcal mol^{-1}). This suggests a weaker interaction between the cyano group of benzonitrile and the zeolite acid sites. Two acids site locations are proposed based on cal-ad results. One strong acid site (site 1, Figure 4-19) is located in the supercage (~ 13 Å) where probes can have access through the 7.4 Å opening. A second strong acid site (site 3, Figure 4-19) is located inside the sodalite cage where the access is not possible because the openings are only 2.4 Å. Proton transfer to strong bases can occur forming an intimate ion pair to the cation in the supercage. Hydrogen bonding interactions for second sites with the probes, found by cal-ad, are assigned to site 4 (Figure 4-19). The n-values indicate that pyridine, 2,6-lutidine and benzonitrile access both strong sites. Quinoline and tetrahydrothiophene access only site 1, and 2,6-di-t-butylpyridine only accesses hydrogen bonding sites.

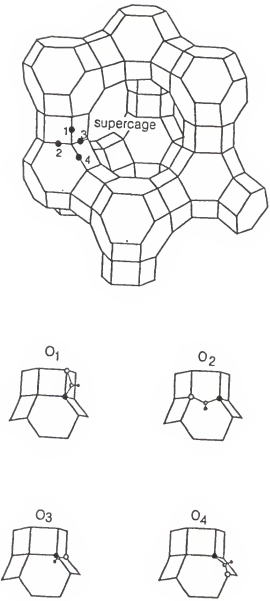

Figure 4-19. Representation of Y zeolite. The corners denote the positions of the T atoms (T = Si or Al) and the lines represent the bridging oxygen atoms. The small pictures show the 4 different positions of the protons that are covalently bonded to the oxygen atoms around an aluminum atom.

The values of ΔH_I from cal-ad for pyridine, quinoline, tetrahydrothiophene and benzonitrile were fit to the following equation to analyze Y zeolite (Si/Al = 6.8) with the ECW model.

$$-\Delta H = E_A E_B + C_A C_B + W$$

where, $E_A E_B$ and $C_A C_B$ describe electrostatic and covalent contributions for the donor (B) -acceptor (A) reaction. The W term is zero for simple donor-acceptor adduct reactions in poorly solvating media. The enthalpies, E_B and C_B values for the donors were substituted into the equation to produce a series of equations that were solved for E_A and C_A. The E_A and C_A values obtained for the strongest site on Y zeolite were 5.25 ± 0.41 and 6.89 ± 0.24, respectively. The C/E ratio (1.31) is higher than for silica gel (1.08) showing that Y zeolite has a stronger covalent character. This is in agreement with the softness character of zeolites suggest by Corma[83] and Fukui.[84] The data fit is shown in Table 4-6. A good fit results showing that the interactions of acid sites and probes for Y zeolite are dominated by donor-acceptor interactions similar to those in solution.

Table 4-6. E and C Fit for the Most Acidic Sites on Y Zeolite (Si/Al = 6.8).

Base	$-\Delta H_{EXP}$ (kcal/mol)	$-\Delta H_{ECW}$ (kcal/mol)	Deviation(kcal/mol)
Pyridine	34.1	33.7	0.4
Benzonitrile	13.2	13.8	0.6
Quinoline	32.1	31.9	0.3
Tetrahydrothiophene	29.0	29.4	0.4

Conclusions

Two types of acid site on Y zeolites have been found by cal-ad and infrared studies. The experimental data over the concentration range employed are fit by cal-ad using a two-site model for pyridine, 2,6-lutidine, quinoline, tetrahydrothiophene and benzonitrile. For 2,6-di-t-butylpyridine a one-site model shows better results and indicates that site 1 is not accessed by this donor.

Cal-ad studies of the reactions of Y zeolite (Si/Al = 6.8) with pyridine and 2,6-lutidine are interpreted by locating the strongest sites (n_1 = 0.1 millimoles g^{-1}) in the large cages of Y zeolite. Approximately 0.2 millimoles g^{-1} of hydrogen bonding sites are also located on the interior and exterior surface of the solid. Comparison of the enthalpy of interaction with pyridine for the first site of Y (ΔH_1 = 34.1 kcal mol^{-1}) and HZSM-5 (ΔH_1 = 42.1 kcal mol^{-1}) shows that Y zeolite is a weaker acid than HZSM-5.

The enthalpies of reactions for the strongest site were well correlated to the ECW model, leading to a large amount of covalent character (C_A/E_A= 1.31) in the donor-acceptor interactions of Y zeolite, which is consistent with literature reports of softness for this zeolite.

LIST OF REFERENCES

1. Cronstedt, A. F. *Sven. Veten. Akad. Hand.* **1756**, 17, 120.

2. Higgins, J.B. *Reviews in Mineralogy*; Heaney, P. J. Prewitt, C. T., Gibbs, G. V., eds., vol. 29, Mineralogical Society of America, Washington, **1994**, 508.

3. Izumi, Y.; Urabe, K.; Onaka, M. *Zeolite, Clay, and Heteropoly Acid in Organic Reactions*; VCH Publishers, Tokyo, **1992**, 10.

4. Dyer, A. *Uses of Natural Zeolites*; Chemistry and Industry, 214.

5. *Zeolites* - Annual Review, by U. S. Dept. of the Interior - Bureau of Mines, **1994**.

6. Milton, R. M. *U. S. Patents* **1959**, 2,882,243 and 2,882,244.

7. Plank, C.J.; Rosinski, E. J. *U. S. Patents* **1964**, 3,140,251.

8. Naccache, C.; BenTaarit, Y. *Pure and Appl. Chem.* **1980**, 52, 2175.

9. Chang, C. D.; Silvestri, A. J. *J. Catal.* **1977**, 47, 249.

10. Davis, M. E.; Suib, S. L. *Selectivity in Catalysis, ACS Symp. Series*, 517, New York, **1991**, 206.

11. Grasselli, R. K.; Brazdil, J. F. *Solid State Chemistry in Catalysis, ACS Symp. Series*, 279, Washington, **1985**, 257.

12. Gabelica, Z.; Derouane, E. G.; Biom, N. *Catalytic Materials, ACS Symp. Series*,

248, Washington, **1984**, 219.

13. Barrer, R. M. *Hydrothermal Chemistry of Zeolites*, Academic Press, London, **1982**.

14. Breck, D. W. *Zeolite Molecular Sieves*, Wiley and sons, New York, **1974**, 305.

15. Kokotailo, G. T.; Lawton, S. L.; Olson, D. H.; Meier, M. W. *Nature* **1978**, 272, 437.

16. Chu, P. *U. S. Patents* **1972**, 3,709,979.

17. McBain, J. W. *The Sorption of Gases and Vapors by Solids*; Rutledge, London, **1952**.

18. Kim, J. H.; Namba, S.; Yashima, T. *Zeolites* **1991**, 11, 59.

19. Hammett, L. P.; Deyrup, A. J. *J. Am. Chem. Soc.* **1932**, 54, 2721.

20. Tanabe, K. *Solid Acid and Bases, Their Catalytic Properties*; Academic Press, New York, **1970**.

21. Sharma, S. B.; Meyers, B. L.; Chen, D. T.; Miller, J.; Dumesic, J. A. *Appl. Catal. A* **1993**, 102, 253.

22. Tanabe, K.; Misono, M.; Ono, Y.; Hattori, H. *Stud. Surf. Sci. Catal.* **1989**, 51, 6.

23. Cvetanovic, R. J.; Amenomiya, Y. *Catal. Rev.* **1972**, 6, 21.

24. Farneth, W. E.; Gorte, R. J. *Chem. Rev.* **1995**, 95, 615.

25. Lim, Y.; Drago, R. S.; Batich, M.; Wong, N.; Doan, P. *J. Am. Chem. Soc.* **1987**, 109, 169.

26. Corma, A. *Chem. Rev.* **1995**, *95*, 559.

27. Plank, C. J.; Rosinski, R. M. *U. S. Patents* **1979**, 4,175,114.

28. van Koningsveld, H.; Jansen, J. C., van Bekkum, H. *Zeolites* **1990**, 10, 235.

29. Guisnet, M. R. *Acc. Chem. Res.* **1990**, *23*, 392.

30. Carniti, P.; Gervasini, A.; Auroux, A. *J. Catal.* **1994**, *150*, 274.

31. Chronister, C. W.; Drago, R. S. *J. Am. Chem. Soc.* **1993**, *115*, 793.

32. a. Nozari, M. S.; Drago, R. S. *Inorg. Chem.* **1972**, 11, 280.

b. Nozari, M. S.; Drago, R. S. *J. Am. Chem. Soc.* **1972**, 94, 6877.

c. Drago, R. S.; Cundari, T. R.; Ferris, D. C. *J. Org. Chem.* **1989**, *54*, 1042.

d. Drago, R. S.; Ferris, D. C.; Wong, N. *J. Am. Chem. Soc.* **1990**, *112*, 8953.

33. a. Parrillo, D. J.; Lee, C. J.; Gorte, R. J. *Appl. Catal. A* **1994**, 110, 67.

b. Farneth, W. E.; Gorte, R. J.; Parrillo, D. J. *J. Am. Chem. Soc.* **1993**, *115*, 12441.

c. Biaglow, A. I.; Gorte, R. J.; Kokotailo, G. T.; White, D. *J. Catal.* **1994**, 148, 779.

d. Lee, C.; Parrillo, D. J.; Gorte, R. J.; Farneth, W. E. *J. Am. Chem. Soc.* **1996**, 118, 3262.

34. Drago, R. S. *Applications of Electrostatic-Covalent Models in Chemistry*; Surfside Scientific Publishers: Gainesville, 1994.

35. a. Batamack, P.; Doremieux-Morin, C.; Fraissard, J.; Freude, D. *J. Phys. Chem.* **1991**, *95*, 3790.

b. Klinowski, J. *Colloids and Surfaces* **1989**, 36, 133.

36. a. Jacobs, P. A.; von Ballmoos, R. *J. Phys. Chem.* **1982,** 86, 3050.

b. Farneth, W. E.; Roe, D. C.; Kofke, T. J. G.; Tabak, C. J.; Gorte, R. J. *Langmuir* **1988**, 4, 152.

37. a. Sauer, J. *Science* **1996**, 271, 774.

b. Smith, L.; Cheetham, A. K.; Morris, R. E.; Marchese, L.; Thomas, J. M.; Wright, P. A.; Chen, J. *Science* **1996**, 271, 799.

38. a. Brand, H. V.; Curtiss, L. A.; Iton, L. E. *J. Phys. Chem.* **1992**, *96*, 7725.

b. Schroder, K. P.; Sauer, J.; Leslie, M.; Catlow, C. R. A.; Thomas, J. M. *Chem. Phys. Lett.* **1992**, 188, 320.

39. a. Cardona-Martinez, N.; Dumesic, J. A. *Adv Catal* **1992**, 38, 149.

b. Yaluris, G.; Larson, R. B.; Kobe, J. M.; Gonzalez, M. R.; Fogash, K. B.; Dumesic, J. A. *J. Catal.* **1996**, *158*, 336.

c. Chen, D. T.; Sharma, S. B.; Filimonov, I.; Dumesic, J. A. *Catal. Lett.* **1992**, 12, 201.

40. Healy, M. H.; Wieserman, L. F.; Arnett, E. M.; Wefers, K. *Langmuir* **1989**, *5*, 114.

41. Derouane, E. G. *Zeolite: Science and Technology*; NATO ASI Series, F. R. Ribeiro et al Eds, 1984, 347.

42. Saito, A.; Foley, H. C. *Microporous Materials* **1995**, 3, 543.

43. Drago, R. S.; McGilvray, J. M.; Webster, C. E. *accepted for publication.*

44. a. Srinivasan, R.; Keogh, R. A.; Ghenciu, A.; Farcasiu, D.; Davis, B. H. *J. Catal.* **1996**, *158*, 502.

b. Wan, K. T.; Khouw, C. B.; Davis, M. E. *J. Catal.* **1996**, *158*, 311.

45. Datka, J.; Boczar, M.; Gil, B. *Langmuir* **1993**, *9*, 2496.

46. Redondo, A.; Hay, P. J. *J. Phys. Chem.* **1993**, 97, 11754.

47. Drago, R. S.; Hirsch, M. S.; Ferris, D. C.; Chronister, C. W. *J. Chem. Soc. Perkin Trans. 2*, **1994**, 219.

48. Farcasiu, D.; Ghenciu, A. *J. Am. Chem. Soc.* **1993**, 115, 10901.

49. a. Haw, J. F.; Nicholas, J. B.; Xu, T.; Beck, L. W.; Ferguson, D. B. *Acc. Chem. Res.* **1996**, 29, 259.

b. Beck, L. W.; White, J. L.; Haw, J. F. *J. Am. Chem. Soc.* **1994**, 116, 9657.

50. Suib, S. L. *Chem. Rev*. **1993**, 93, 803.

51. Taramasso, M.; Perego, G.; Notari, B. *U.S. Patent* **1983**, 4, 410, 501.

52. Meier, W.M.; Olson, D.H. *Atlas of Zeolite Structure Types,* Butterworth-Heinemann, **1992**, 138.

53. Thangaraj, A.; Kumar, R.; Mirajkar, S.P.; Ratnasamy, P. *J. Catal.* **1991**, 130, 1.

54. Mirajkar, S.P.; Thangaraj, A.; Shiralkar, V.P. *J. Phys. Chem.* **1992**, 96, 3073.

55. Notari, B. *Catalysis Today* **1993**, 18, 163.

56. Grzybowska-Swierkosz, B.; Haber, J. *Annual Reports on the Progress of Chemistry*, Section C, **1994**, 91, 403.

57. Notari, B. *Advances in Catalysis*, **1996**, 41, 253.

58. Boccuti, M. R.; Rao, K. M.; Zecchina, A.; Leofanti, G.; Petrini, G. *Stud. Surf. Sci.*

Catal., **1989**, 48, 133.

59. Bellussi, G.; Carati, A.; Clerici, M.G.; Maddinelli, G.; Millini, R. *J. Catal.* **1992**, 133, 220.

60. Corma, A.; Esteve, P.; Martinez, A. *J. Catal.* **1996**, 161, 11.

61. Klein, S.; Maier, W. F. *Angew. Chem. Inter. Ed. Engl.* **1996**, 35, 2230.

62. Chen, M. C.; Chu, S. J.; Chang, N. S.; Chen, P. Y.; Chang, T. K.; Chen, L. Y. *Catalysis* **1989**, Ward, J. W., eds; Elsevier, Amsterdam, 253.

63. Kulkarni, S. B.; Shiralkar, V. P.; Kotasthane, A. N.; Borade, R. B.; Ratnasamy, P. *Zeolites* **1982**, 2, 313.

64. Toba, M.; Mizukami, F.; Niwa, S.; Sano, T.; Maeda, K.; Annila, A.; Komppa, V. *J. Mol. Catal.* **1994**, 91, 277.

65. Liu, Z.; Tabora, J.; Davis, R. J. *J. Catal.* **1994**, 149, 117.

66. Drago, R.S.; Dias, S.C.; Torrealba, M.; Lima, L. *J. Am. Chem. Soc.* **1997**, 119, 4444.

67. Drago, R.S.; Dias, S. C.; McGilvray, J. M.; Mateus, A. L. *J. Phys. Chem.* acceptted for publication.

68. Rabo, J. A.; Pellet, R. J.; Risch, A. P.; Blackwell, C. S. *8th Annual Fluid Catal. Cracking Symposium* **1987**, Budapest, Hungary.

69. Upson, L. L. *8th Annual Fluid Catal. Cracking Symposium* **1987**, Budapest, Hungary.

70. Focus on Catalysts, The Royal Society of Chemistry, Cambridge, UK, 1, **1993**.

71. Barrer, R. M.; Makki, M. B. *Can. J. Chem.* **1964**, 42, 1481.

72. Kerr, G. T. *J. Catal.* **1969**, 15, 200.

73. Scherzer, J. *J. Catal.* **1978**, 54, 285.

74. Scherzer, J. *Catal. Rev.-Sci. Eng.* **1989**, 31, 215.

75. Stucky, G. D. *Progress in Inorganic Chemistry*, vol. 40, Interscience Publication, Ed. by Stephen J. Lippard, **1992**.

76 Breck, D. W. *Zeolite Molecular Sieves*, Wiley, Mew York, **1974**.

77. Scherzer, J.; Bass, J. L.; Hunter, F. G. *J. Phys. Chem.* **1975**, 79, 1194.

78 Kasai, P.H.; Bishop, R. J. *Zeolite Chemistry and Catalysis*, ACS Symposium, J. A. Ed., **1971**, 171, 350.

79. Macedo, A.; Auroux, A.; Raatz, F.; Jacquinot, E.; Boulet, R. *Perspectives in Molecular Sieve Science*, ACS Symposium, **1988**, 98.

80. Biaglow, A. I.; Parrillo, D. J.; Gorte, R. J. *J. Catal.* **1993**, 144, 193.

81. Williams, K. R. *J. Radioanal. Nucl. Chem., Letters* **1996**, 212, 361.

82. Ingamells, C. O. *Anal. Chim. Acta.* **1970**, 52, 323.

83. Corma, A.; Llopis, F.; Viruela, P.; Zicovich-Wilson, C. *J. Am. Chem. Soc.* **1994**, 116, 134.

84. Parr, R. G.; Yang, W. *J. Am. Chem. Soc.* **1984**, 106, 4049.

BIOGRAPHICAL SKETCH

Sílvia C. L. Dias was born in Fortaleza, a city located in the state of Ceará, northeast of Brazil on March 2, 1967, to parents Ubatan and Maria Loureiro. She attended Leonardo da Vinci High School in Brasília, Distrito Federal and graduated in December 1983. In July of 1984 she began college at the Universidade de Brasília, Brazil as a chemistry major. She married José A. Dias on February 27th, 1987. She graduated in July of 1989 with B.S degree.

She entered graduate school at the Department of Chemistry in the Universidade de Brasília, Brazil in August of 1989. Her thesis title was "Equilíbrios e Estruturas dos Complexos de Ferro (III) com Ácido Glicólico em Meio Aquoso." She graduated with a M. S. in Chemistry under the direction of Dr. David P. Geeverghese in August 1992.

In May 1993, she was approved, based on a written and a public oral qualifing exam, to work as full Professor in the Department of Chemistry at the Universidade de Brasília, Brazil.

In January 1994, she began graduate school at the University of Florida to attain her doctorate in chemistry under the direction of Dr. Russell S. Drago. Her research has focused on characterization of zeolites and zeotypes.

The author has published a paper, submitted a second one, and is currently working on a third one. Upon receiving the degree of Doctor of Philosophy, she will return to the Universidade de Brasília, Brazil as Associate Professor, where she intends to teach and develop research.

I certify that I have read this study and that in my opinion it conforms to acceptable standards of scholarly presentation and is fully adequate, in scope and quality, as a dissertation for the degree of Doctor of Philosophy.

Dr. Russell S. Drago, Chair
Graduate Research Professor of Chemistry

I certify that I have read this study and that in my opinion it conforms to acceptable standards of scholarly presentation and is fully adequate, in scope and quality, as a dissertation for the degree of Doctor of Philosophy.

Dr. Daniel R. Talham
Associate Professor of Chemistry

I certify that I have read this study and that in my opinion it conforms to acceptable standards of scholarly presentation and is fully adequate, in scope and quality, as a dissertation for the degree of Doctor of Philosophy.

Dr. David E. Richardson
Professor of Chemistry

I certify that I have read this study and that in my opinion it conforms to acceptable standards of scholarly presentation and is fully adequate, in scope and quality, as a dissertation for the degree of Doctor of Philosophy.

Dr. Samuel O. Colgate
Professor of Chemistry

I certify that I have read this study and that in my opinion it conforms to acceptable standards of scholarly presentation and is fully adequate, in scope and quality, as a dissertation for the degree of Doctor of Philosophy.

Dr. Joseph H. Simmons
Professor of Materials Science Engineering

This dissertation was submitted to the Graduate Faculty of the Department of Chemistry in the College of Liberal Arts and Sciences and to the Graduate School and was accepted as partial fulfillment of the requirements for the degree of Doctor of Philosophy.

December, 1997

_____

Dean, Graduate School